The comparative effect of HMX content on the detonation performance characterization of PBX 9012 and PBX 9501 high explosives

Eric K. Anderson, Carlos Chiquete*, Scott I. Jackson, Ritchie I. Chicas, Mark Short

Los Alamos National Laboratory
Los Alamos, NM 87545

Abstract

A series of detonation performance experiments are described for the plastic-bonded high explosive (HE) PBX 9012, nominally composed of 90% octahydro-1,3,5,7-tetranitro-1,3,5,7-tetrazine (HMX) and 10% polymeric binder vinylidene-hexafluoropropylene copolymer (Viton VTR-5883), by weight. The experiments provide information on the PBX 9012's detonation propagation properties and metal pushing characteristics. Although this HE formulation has been in use for 50 years as a booster (compositionally similar to LX-07), our new data represent the first full detonation performance characterization for the HE (along with recently reported shock initiation experiments). Here, we compare the new PBX 9012 data with the well-studied PBX 9501 (95% HMX and 5% polymeric binder), establishing how the 5% difference in HMX content between the explosives is manifested in the performance measurements. A scaling argument based on the known energetic material content in a large selection of high HMX content formulations is also given to help explain the observed results. Finally, the accumulated PBX 9012 data is used to generate performance models using both programmed and reactive burn techniques, providing an additional avenue to compare PBX 9012 to the more energetic PBX 9501.

Keywords: detonation performance, calibration, reactive burn, programmed burn, HMX, high explosive

1. Introduction

The high-performance plastic-bonded high explosive (HE) PBX 9012 is nominally composed (by weight) of 90% octahydro-1,3,5,7-tetranitro-1,3,5,7-tetrazine (HMX) and 10% polymeric binder vinylidene-hexafluoropropylene copolymer (Viton VTR-5883). It is primarily intended as a booster for initiation of insensitive main charges in explosive systems. Many explosives with varying levels of HMX percentage and different binder materials have been formulated and characterized. Of most relevance, the Lawrence Livermore National Laboratory explosive LX-07 has the same nominal formulation as PBX 9012 but is pressed to a higher density, specifically 1.860-1.870 g/cm^3 for LX-07 compared to 1.845 $\pm$ 0.005 g/cm^3 for PBX 9012 [1–3]. Recently,

the shock-to-detonation transition of PBX 9012 was investigated with plate impact experiments and modern embedded gauge diagnostics to reveal the reaction zone profile as the detonation develops in the HE [4], thus providing a shock sensitivity comparison between the two explosives. The current work describes detonation propagation experiments in axisymmetric cylindrical geometries ("rate sticks") and a cylinder expansion test (CYLEX) equipped with Photon Doppler Velocimetry (PDV) for the PBX 9012 formulation. Along with [4], this completes a full characterization of this HE's detonation performance, providing the data required for model parameterization and subsequent predictive calculations to facilitate engineering design.

As noted, there are a number of HMX-based explosives related to PBX 9012. One of the most studied of these is PBX 9501, composed of 95% HMX, 2.5% polyester urethane random copolymer (Estane), and 2.5% of a eutectic mixture of bis(2,2-dinitropropyl)acetal and bis(2,2-dinitropropyl)formal (BDNPA/BDNPF). In addition to the binder material difference, the HMX content in PBX 9012 is 5% less than in PBX 9501 and additionally, the pressing density differs between the explosives (1.845 compared to 1.83 g/cm^3 for PBX 9501). The HMX content, binder material and pressing density are known to affect the detonation performance characteristics of HEs including the detonation wave velocity and the ability of the explosive to accelerate surrounding materials. Given that analogous data exists for PBX 9501 for every PBX 9012 measurement obtained here, an additional objective of our work is to analyze the comparative performance effect of the formulational differences between the explosives. In particular, scaling relationships are sought to relate the measured performance data for the two explosives. Additionally, a scaling analysis based on HMX content is also performed to highlight relationships between the performance characteristics of a larger selection of high HMX-content formulations and add context to our PBX 9012-PBX 9501 comparisons. The detonation performance model calibration of the accumulated data is also pursued to provide a further avenue to compare the explosives beyond the new experimental measurements as well as new simulation tools for PBX 9012. Of particular interest, model properties such as the reaction zone and equation of state (EOS) for the product gases can then be compared between the two explosives.

Two relevant categories of detonation performance models exist for condensed high explosives and are both used here to help characterize PBX 9012. In the Reactive Burn (RB) approach, a (finite) reaction rate dictates the conversion of unreacted solid HE to product gas. The RB model EOSs for both reactants and products and reaction rate are based on empirical forms and calibrated to experiment. These assembled components then generate a model representation of the HE reaction zone (RZ). However, RB methods have computational constraints due to the fine RZ scales (in relation to the much larger engineering geometry counterparts) that must be resolved to accurately describe the detonation propagation and accompanying energy release. These stringent resolution requirements led to the early adoption and continued use of more efficient Programmed Burn (PB) models which separately calculate the detonation wave motion and the energy release behind the front.

This paper is laid out as follows: we first report on the performance experiments we use to characterize PBX 9012. The experimental data for PBX 9012 is then compared to equivalent data for PBX 9501 and a new scaling relation is derived to estimate the detonation performance properties of high HMX content HEs. We describe how this data is used to yield programmed burn and reactive flow model calibrations. Many of the descriptions of models and numerical approaches we use here are similar to those recently used to characterize other plastic-bonded explosives [5, 6].

2. Experiments

The detonation performance experiments for PBX 9012 consisted of five front-curvature unconfined rate sticks at varying diameters and one cylinder expansion test (CYLEX). These tests generate a steady detonation wave in the axisymmetric two-dimensional geometry, which allows for measurement of the resulting detonation velocity, detonation front shape, RZ structure, and the accessed range in the products equation of state. Varying the charge diameter modulates these parameters as it influences the relative strength of the fluid mechanical flow expansion in the reaction zone, which in turn affects the detonation shock strength and chemical energy release [7, 8]. These data are then used to calibrate programmed and reactive burn models [9], which are able to predict the evolution of the detonation in more complex geometries. The experimental methodologies used in the present study are consistent with our prior works [5, 6, 10] and are detailed below.
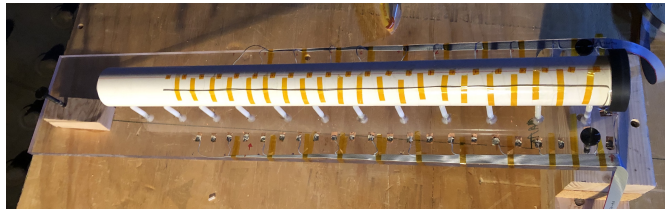
2.1. Test Geometries

Figure 1: Front-curvature rate stick 8-2173 with the detonator at left and the breakout window on the right.

Front-curvature rate sticks are used to characterize detonation velocity and front shape variations with charge diameter. The test consists of a large-aspect-ratio explosive rod that is sufficiently long to damp out any initiation transients and generate a steady detonation wave in the measurement region [7]. In the present study, five unconfined PBX 9012 rate sticks were fielded with diameters of 50, 10, 6 and 4 mm. A charge length-to-diameter ratio (L/d) of 12 was used for diameters of 10.2 mm and larger, which is long enough for conventional explosives to relax from the initiator and achieve steady state [11]. An L/d ratio of 24 was used for smaller diameter tests.

It is difficult to machine a long rod of PBX 9012 with the necessary tolerances so instead, each rate stick was composed of 12 explosive pellets as shown in Fig. 1. Each pellet was uniaxially pressed into the form of a right circular cylinder with an aspect ratio of $L/d = 1$ or 2. These L/d ratios minimize the presence of density gradients in the individual pellets. Pellet densities as measured via immersion densitometry and dimensions are reported in this paper's supplementary materials. The pellets were then glued together in order of increasing density from the initiator end. AngstromBond 9110LV epoxy was used under pressure to achieve glue joint thicknesses of less than 10 μm. All rate sticks were initiated directly with a Teledyne RISI RP-1 detonator, supported with plastic assemblies, and instrumented with both ionization probes and front shape mirror diagnostics as described below.

The cylinder expansion test [12] consisted of an inert confiner tube tightly encasing the assembled rod of PBX 9012 explosive, as shown in Fig. 2. The tube was composed of Oxygen-Free High-Conductivity (OFHC) copper annealed to a dead-soft temper. The test scale was a standard 1-inch cylinder test [13] with an outer diameter of 30.49 mm, an inner diameter of 25.44 mm,

Identifier	Type	d	L/d	ρ_0	D_0
		(mm)		(g/cc)	(mm/μs)
8-2173	FC	50.7	12.0	1.841	8.585±0.002
8-2226	FC	50.7	12.0	1.842	8.58±0.0013
8-2169	FC	10.2	11.9	1.844	8.573±0.003
8-2170	FC	5.7	23.9	1.847	8.533±0.005
8-2171	FC	3.9	24.2	1.844	8.512±0.004
8-2172	CYLEX	25.4	12.0	1.843	8.582±0.003

Table 1: PBX 9012 experimental test types, diameter, average initial explosive density (ρ_0), and measured detonation velocity (D_0). "FC", and "CYLEX" indicates front curvature and detonation velocity, and cylinder expansion test, respectively.

a wall thickness of 2.53 mm, and a length of 305 mm. The concentricity of the inner and outer diameters were measured and verified to be concentric to within 0.005 mm.

Twelve explosive pellets of PBX 9012 with an outer diameter of 25.4 mm and an L/d of unity were inserted into the cylinder to fully fill it. Pellet joints and the small gap between the cylinder inner diameter and the explosive were filled with Sylgard 184 silicone elastomer to secure the explosive and prevent jetting. Individual pellet densities, diameters, and lengths are shown in Table 1. Eight collimated PDV probes were used to measure the motion of the wall during the experiment. The PDV probes were oriented normal to the initial cylinder wall orientation to generate the most direct measurement of the wall motion [14] for subsequent analysis. Probes were located at two axial distances from the detonator–explosive interface, 204 mm and 229 mm, corresponding to $0.67L_t$ and $0.75L_t$ where L_t is the total length of the charge, respectively. Each probe was placed at a different azimuthal location, 90 degrees apart as shown in Fig. 2. PDV1-4 were located at 0.67 L_t with azimuthal angles of 0, 90, 180, and 270°, respectively. PDV5-8 were located at 0.75 L_t with azimuthal angles of 0, 90, 180, and 270°, respectively. In similar fashion to the rate stick tests, the cylinder test was directly initiated from a Teledyne RISI RP-1 detonator and equipped with both shorting wires and a front shape mirror as described below.

The axial charge length in the direction of detonation propagation must be sufficiently long that a steady two-dimensional detonation velocity can be achieved. Typically, this requires a length of several charge thicknesses (2-4) to both damp out any booster overdrive or underdrive and allow for the two-dimensional flow to be established. A length of 12 diameters is the standard [11]. Additionally, the explosive reaction zone length (RZL) can affect the relaxation to steady propagation (explosives with longer RZLs take longer to become steady) and thus we aim to have at least 1000 reaction zone lengths per rate stick length. For this reason, the smaller diameter tests have longer aspect ratios to maintain the RZL criterion [7].

2.2. Diagnostics

Ionization probes, as described in [7], were used to characterize the detonation phase velocity D_0 at the rate stick outer radius. Each rate stick was instrumented with 11 ionization probes, except the 50.7 mm diameter tests which were instrumented with 22 probes. The cylinder test was similarly instrumented, however the probes were set up to operate as shorting wires for this test as they transmitted current to the tube (acting as a ground as described below) instead of through the detonation reaction zone. The first probe was located at an axial distance of $2d$ from the detonator–explosive interface. The other probes were equidistantly spaced over the remaining
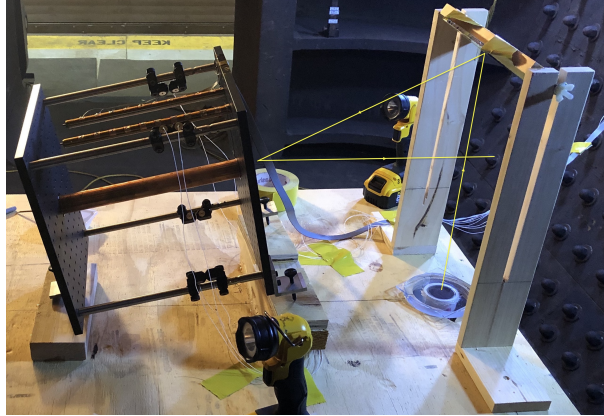
Figure 2: Cylinder test 8-2172 with the detonator at left, breakout window at right. The yellow lines show the light path from the argon flash (inset into the assembly support table) to the front surface window to the streak camera (off image, to the right).

$10d$. Each probe consisted of a 50.2-μm-diameter (44-AWG) coated copper magnet wire bent into a chevron shape, with the tip located along a line parallel to the axial charge centerline so that the detonation would first contact this tip. Each wire was raised to an electrical potential of 75.0 V through use of an RC circuit. For rate sticks, a single, thicker copper grounding wire was located on a line parallel to the axial centerline of the opposing charge surface. For the cylinder test, the copper tube served as the ground. Arrival of the ionization front associated with the detonation wave at each probe vaporized the thin enamel coating and allowed current to flow from the high-voltage wire to ground, resulting in a measured voltage spike associated with current flow from the 75V wire to the ground wire (via an RC circuit). Similarly, for the cylinder test, the arrival of the incident shock at the cylinder wall allowed for the insulated wire to short to the wall, generating current flow. Probe locations were measured to better than 30 μm and the pin voltage was sampled with a bandwidth of 1 GHz (5 GS/s sample rate) during each test. Probe position and detonation arrival time data were fitted to a line using a least-squares fit optimization. The slope of the line was the steady-state detonation velocity D_0. These velocities are reported in Table 1 along with the standard error (SE) associated with the fit to D_0.

The detonation front shape was recorded at the breakout surface of the downstream pellet using a mirror destruction technique [15]. A PMMA window was glued over the downstream pellet face and a diameter chord of the window was coated with a 0.4-μm-thick aluminum layer (Fig. 3). During the experiment, light was directed from an argon flash [16] to this aluminum layer (Fig. 2). That light was then specularly reflected to a Cordin 131 streak camera. Arrival of the detonation at the downstream face destroyed the aluminum surface and cut off the reflected light, allowing the shape of the detonation to be recorded at the breakout face.

The PDV probes used for the cylinder test were collimated with a 100-mm working distance and a spot size of less than 350 μm. Each probe was located approximately 150 mm from the initial cylinder wall location. The portion of the cylinder wall that was observed by each probe was sanded with scotchbrite to generate diffuse reflectivity. PDV data was recorded at a bandwidth of 20 GHz (50 GS/s digitizer rate) and reduced using a 32-bit Fourier window size and a 4096-bit window step size.
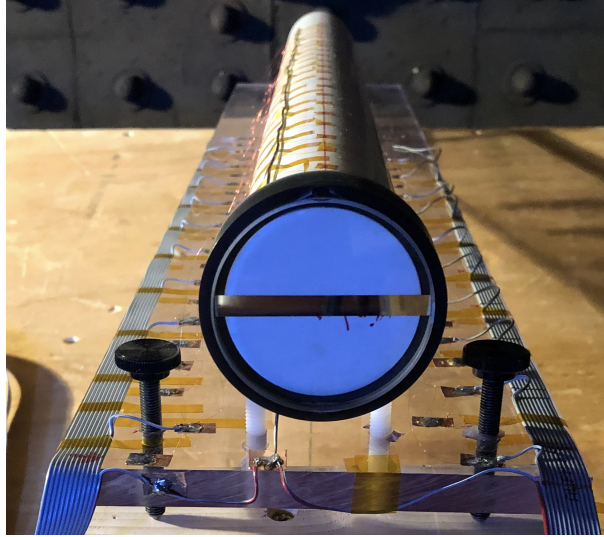
Figure 3: The window on the breakout surface of test 8-2173.

3. Experimental results and scaling analysis

3.1. Phase velocity and curvature

Figure 4 shows the phase velocity and front curvature data from the PBX 9012 rate stick and CYLEX tests (see also Table 1). The data manifests the well-known "diameter effect" on the propagation properties of detonations in finite-sized charges. The steady-state velocity decreases as R decreases (Fig. 4a) while generating increased curvature across the front (see Fig. 4b). The phase velocity for the CYLEX test does not appear to include an effective confinement due to the thickness (approximately 35 μm) of the Sylgard layer between the HE and the inner surface of the Cu layer (see section 2.1).

To add context to the PBX 9012 experimental results in Fig. 4a, Fig. 5 compares the present unconfined geometry data to equivalent data for PBX 9501 [7]. There is an evident drop in PBX 9012 detonation velocity of about 200 m/s relative to PBX 9501, seemingly uniform for the shown range of charge diameters. If the data is plotted on a vertical axis normalized by each HE's Chapman-Jouguet velocity (D_{CJ}), where we have used $D_{CJ}^{9501} = 8.79$ mm/μs [17] and $D_{CJ}^{9012} = 8.59$ mm/μs as determined in section 4.1.1, the entirety of the data collapses onto the same general curve (Fig. 6). This result implies that there is a multiplicative factor that relates the diameter effects of the two explosives,

$$\begin{aligned} D_0^{9501} &\approx D_0^{9012} \times D_{CJ}^{9501}/D_{CJ}^{9012}, \\ &\approx D_0^{9012} \times 1.023, \end{aligned} \tag{1}$$

where D_0 denotes the phase velocity for a given charge-size and the superscript refers to the specific HE. There are several apparent implications that should be highlighted: the first order effect of reducing the HMX content on the diameter effect appears to be an overall reduction in the energy available for propagation and it applies uniformly regardless of charge size (at least for the available range of data). As described previously, the velocity deficit (relative to

6
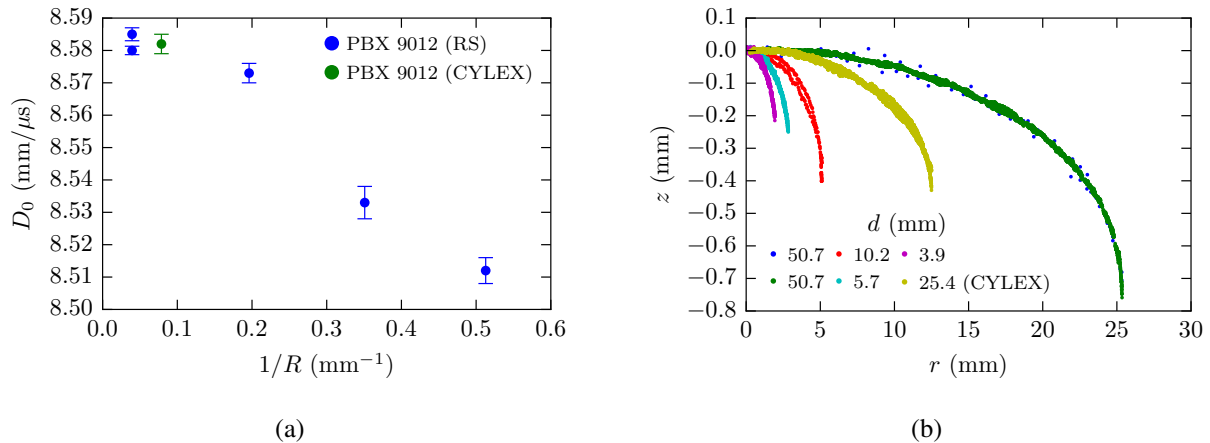
Figure 4: (a) Diameter effect data (D_0 vs. $1/R$, where $R = d/2$ is the radius of the charge) produced in the five rate sticks and single CYLEX test with experimental error bars. (b) Front shape variations showing detonation shock deflection (z) as function of radial coordinate (r) for each test.

D_{CJ}) for a given charge size depends on the interaction of the chemical reaction zone kinetics, fluid mechanics of the imposed flow divergence and resulting loss of energy for propagation. Therefore, the energy loss for a given charge size must be proportionally the same between PBX 9012 and PBX 9501 since the velocity decrement itself is also proportionally similar. We therefore contend that the energy release profile should be similar between the explosives, thus implying that the binder material, reduction in HMX content, and different post-shock conditions do not fundamentally affect the chemical kinetic pathways. This specific hypothesis is tested in our RB model calibration described in section 4.2 which produces a rate law and RZ profile that can be usefully compared between PBX 9012 and PBX 9501.

3.2. Confiner wall push

The wall motion measurements from the CYLEX test are presented in Fig. 7 and test details appear in Table 1. The limiting Cu wall velocity for PBX 9012 is close to 1800 m/s. As a reference point, the more energetic PBX 9501 result [18] is presented as well, revealing a difference of about 100 m/s between the explosives for most of the shown range. Note that the PBX 9501 CYLEX test had a Sylgard layer thickness of approximately 17 μm. The minor mass difference associated with the Sylgard layer thickness variation between the PBX 9012 (35 μm) and PBX 9501 CYLEX tests would not account for the significant difference in the Cu wall expansion rates. Of significance, if one scales the PBX 9012 wall velocity by the previously established ratio of CJ detonation speeds as in Fig. 8, the data largely collapses again.

3.3. Scaling analysis

The ratio of the PBX 9012 and PBX 9501 CJ speeds appears critical to collapsing both the PBX 9012 diameter effect and the velocity of the confining Cu wall push close to the equivalent behavior for PBX 9501. In the following, we explore the relationship between this ratio and measurable formulation properties, and investigate whether the CJ speed scale factor has potentially wider implications for a class of HMX-based conventional HEs. A volume V of PBX 9501

7
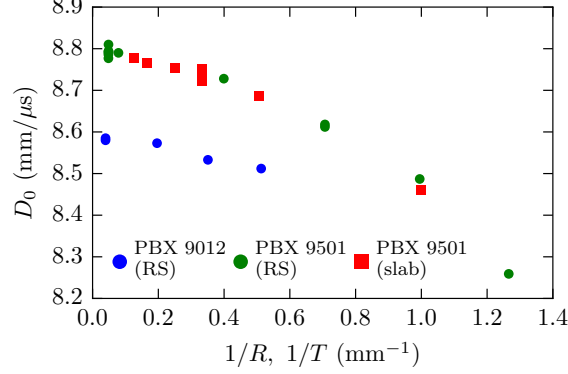
Figure 5: Unconfined diameter effect data for PBX 9012 and size effect (slab and rate stick) data for PBX 9501 [7]. Here, T represents the thickness of the PBX 9501 slab geometry tests.
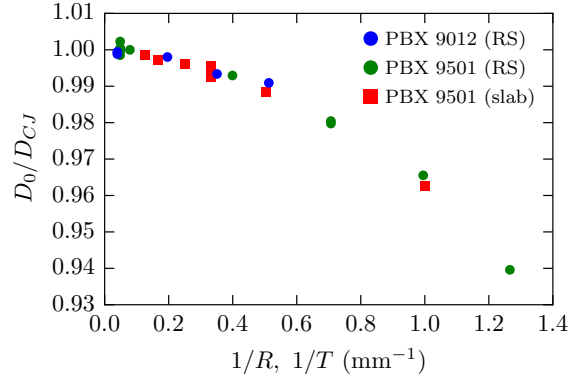
Figure 6: Diameter effect data for PBX 9012 and PBX 9501 but plotted on a dimensionless vertical axis with help of the Chapman-Jouget velocity (D_{CJ}) for each explosive. We have used D_{CJ} values extrapolated from detonation propagation model analysis for each HE, $D_{CJ} = 8.59$ and 8.79 mm/μs for PBX 9012 and 9502, respectively.

(95% HMX and 5% binder by weight with a nominal pressing density $\rho_{0,9501} = 1.830$ g/cm^3) contains an HMX mass,

$$M_{HMX}^{9501} = (w_{HMX}^{9501}/100)\, M_{9501} = (w_{HMX}^{9501}/100)\rho_{0,9501}V, \tag{2}$$

where $M_{9501} = \rho_{0,9501}V$ is the total mass of PBX 9501 in V and w_{HMX}^{9501} is the HMX weight percentage in PBX 9501. Equivalently, for PBX 9012 (90% HMX and 10% binder by weight with a nominal pressing density $\rho_{0,9012} = 1.845$ g/cm^3),

$$M_{HMX}^{9012} = (w_{HMX}^{9012}/100)\rho_{0,9012}V. \tag{3}$$

8
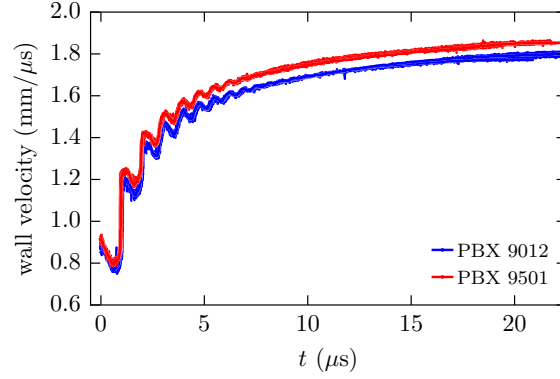
Figure 7: Wall velocity profile for the 25.4 mm diameter PBX 9012 CYLEX test along with an equivalent result for PBX 9501 for a similar geometry [18].
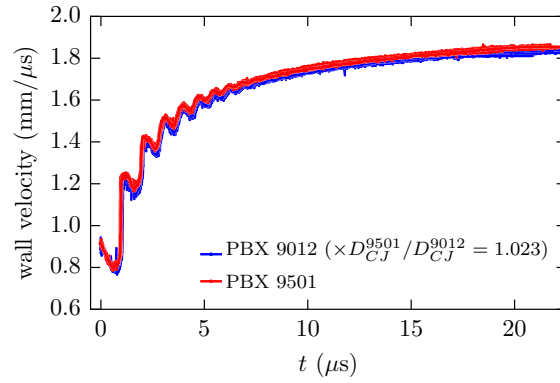
Figure 8: As in Fig. 8 but the PBX 9012 wall motion result has been multiplied by the ratio of CJ speeds between PBX 9012 and PBX 9501.

The ratio of the HMX masses is

$$\frac{M_{HMX}^{9501}}{M_{HMX}^{9012}} = \frac{(95/100)\rho_{0,9501}}{(90/100)\rho_{0,9012}} = \frac{(95/100)(1.83)}{(90/100)(1.845)} \tag{4}$$
$$= 1.04697.$$

However, we also note that from the diameter effect evaluation of D_{CJ} for each HE (see §3.1 and §4.1.1),

$$\left(\frac{D_{CJ}^{9501}}{D_{CJ}^{9012}}\right)^2 = \frac{8.79^2}{8.59^2} = 1.04710, \tag{5}$$

suggesting that for PBX 9501 and PBX 9012,

$$\frac{M_{HMX}^{9501}}{M_{HMX}^{9012}} \approx \left(\frac{D_{CJ}^{9501}}{D_{CJ}^{9012}}\right)^2. \tag{6}$$

9
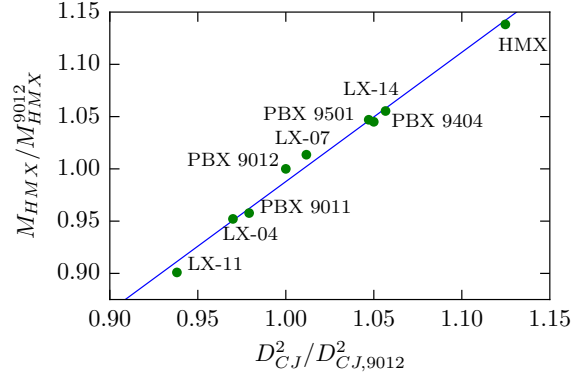
Figure 9: Variation of M_{HMX}/M_{HMX}^{9012} vs. $D_{CJ}^2/D_{CJ,9012}^2$ for a set of HMX-based explosives.

Explosive	HMX (wt. %)	ρ_0 (g/cm^3)	D_{CJ} (mm/μs)	Binder (wt. %)	Source
HMX	100	1.89	9.110		[11]
LX-14	95.5	1.835	8.83	Estane 5702-F1 (4.5%)	[1]
PBX 9501	95	1.830	8.790	Estane (2.5%), BDNPA/BDNPF (2.5%)	[17]
PBX 9404	94	1.846	8.802	NC (3%), CEF (3%)	[11]
PBX 9012	90	1.845	8.590	Viton VTR-5883 (10%)	this work
PBX 9011	90	1.767	8.500	Estane 5703 (10%)	[11]
LX-07	90	1.87	8.640	Viton A (10%)	[1]
LX-04	85	1.86	8.460	Viton A (15%)	[1]
LX-11	80	1.87	8.320	Viton A (20%)	[1]

Table 2: Explosive formulation data used in the HMX-based HE scaling analysis (Fig. 9). The tris-beta-chloroethylphosphate (CEF), Viton- and Estane-based plasticizer materials are considered inert while nitrocellulose (NC) and BDNPA/BDNPF [19] are considered weakly energetic.

This relation suggests that the CJ speed of PBX 9012 can potentially be determined from knowledge of the PBX 9501 CJ speed and the ratio of HMX mass content between PBX 9501 and PBX 9012. It is then of interest to examine whether a similar scaling holds amongst the wider class of HMX-based explosives with high weight percentages of HMX and either inert or weakly energetic binders. Figure 9 shows the ratio of HMX mass to the ratio of D_{CJ}^2, both relative to PBX 9012, for a series of HMX-based HEs. The formulations of these HEs and their HMX and binder weight percentages are given in Table 2. Other than PBX 9501 and PBX 9012, the data used in Fig. 9 is taken from [1, 11] and spans a considerable range of initial pressing densities (1.767–1.89 g/cm^3), HMX content (80-100%) and detonation velocity (8.32–9.11 mm/μs). A linear fit to the variation gives

$$\frac{M_{HMX}}{M_{HMX}^{9012}} = 1.237 \frac{D_{CJ}^2}{D_{CJ,9012}^2} - 0.2490, \tag{7}$$

10

where M_{HMX} is the HMX mass content in a volume V for any of the HEs and D_{CJ} is the corresponding CJ speed. This provides a scaling relationship to approximate the CJ speed of any target HMX-based explosive with inert or weakly energetic binders based on knowledge of the weight percentage of the HMX in the target HE, and of knowledge of the initial pressing density and D_{CJ} of any of the other HEs in Fig. 9. Thus, the scaling (7) can be particularly useful for the development of new HMX-based HE formulations whose detonation performance properties are desired to be greater or less than some existing reference HE formulation.

4. PBX 9012 detonation performance models

We now turn to a series of detonation model calibrations for PBX 9012 based on the performance data described in §2. This enables us to investigate additional scaling relationships between the behavior of PBX 9012 and PBX 9501. Detonation performance modeling at the engineering scale mainly relies on two approaches, namely programmed burn (PB) and reactive burn (RB) [20, 21]. In the following, we calibrate PBX 9012 models for both PB and RB simulation methodologies.

Programmed burn (PB) methods employ sub-scale modeling of the detonation wave motion (timing) combined with a description of the explosive energy release that supports the work done by the detonation products. The latter largely serves to provide the push by the detonation on any surrounding confinement. Programmed burn methods are designed to operate on coarse computational meshes without explicitly resolving the reaction zone spatial and temporal scales. The Detonation Shock Dynamics (DSD) surface propagation model [5, 7, 20, 22, 23], which relates the surface normal speed (D_n) to its local curvature (κ), is used here to calculate the detonation motion for PBX 9012. For the associated energy release component, we use the Pseudo-Reaction-Zone (PRZ) model [24] which improves on prior PB methods by delivering energy in a spatially-distributed reaction zone, after triggering by the DSD timing calculation. Hydrocode simulations are used to simultaneously calibrate the reaction rate and product EOS for the PBX 9012 PRZ model by iterating on the parameters of the reaction rate and product EOS model until the hydrocode simulations closely match the experimentally determined diameter effect and CYLEX test wall motion (§2). For the interested reader, we have also provided a calibrated form of the Jones-Wilkins-Lee (JWL) EOS for PBX 9012 in Appendix A that can be deployed in traditional PB methods.

A reactive burn model is additionally calibrated, specifically a variant of the Wescott-Stewart-Davis (WSD) model [25] with a modified reaction rate term and closure condition. In contrast to PB methods, RB methods can directly incorporate shock initiation effects, in addition to propagation and metal push physics. Reactive burn models inherently couple the timing and energy release components of detonation performance, but in turn generally require spatial and temporal resolution of the fine reaction zone time and length scales to generate accurate performance simulations.

4.1. DSD/PRZ PB model for PBX 9012

4.1.1. Detonation Shock Dynamics calibration

The functional form for the DSD surface propagation law is given by [5, 7, 17],

$$D_n(\kappa) = D_{CJ}\left(1 - B\kappa\frac{1 + C_2\kappa + C_3\kappa^2}{1 + C_4\kappa + C_5\kappa^2}\right), \tag{8}$$

11

(a)	(b)
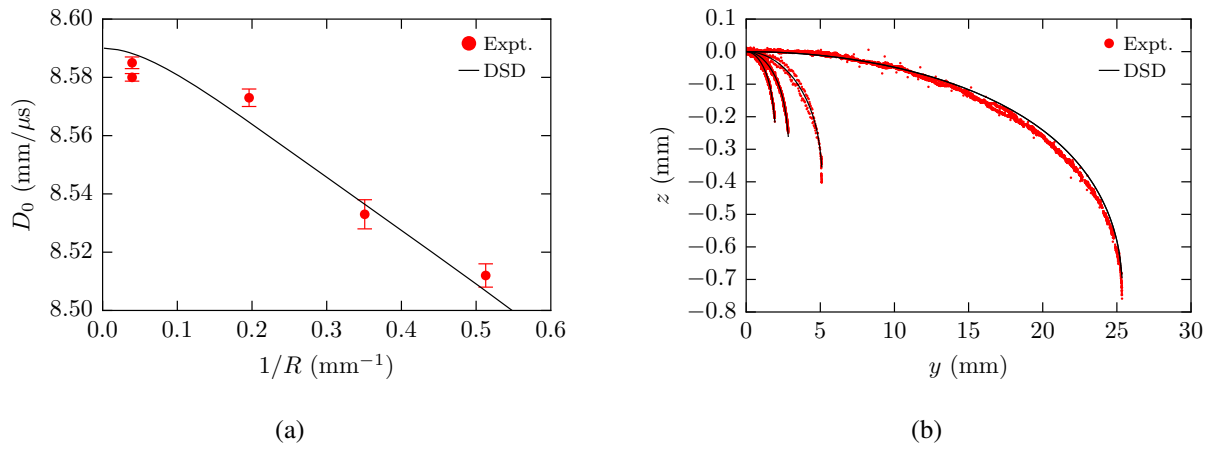
Figure 10: Comparison of (a) experimental diameter effect and (b) front shape data (symbols) to the DSD calculations (curves).

(a)	(b)
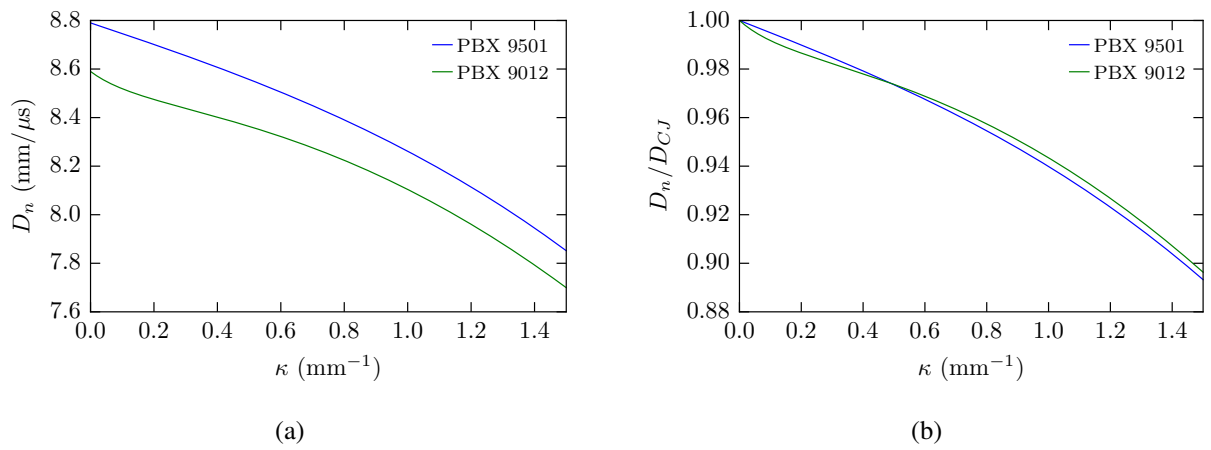
Figure 11: (a) The D_n versus κ variation for PBX 9012, shown with the equivalent model for PBX 9501 [17]. (b) A comparison of $D_n(\kappa)/D_{CJ}$ versus κ using each model's D_{CJ} parameter.

D_{CJ} (mm/μs)	B (mm)	C_2 (mm)	C_3 (mm^2)	C_4 (mm)	C_5 (mm^2)	ϕ_s (deg.)
8.590	0.116	0.229	1.464	4.512	0.000	30.0

Table 3: Optimized DSD propagation law parameters for PBX 9012.

where D_{CJ}, B and C_i for $i = 2, \ldots 5$ are the propagation law parameters. For the rate stick geometry (§2), the DSD model also requires the specification of an edge angle parameter (ϕ_e) which accounts for the effect of HE confinement on detonation motion. Here, ϕ_e represents the angle between the normal to the DSD surface at the confinement interface and the tangent to the confinement surface [17] (note that for unconfined rate sticks, the edge angle takes on its sonic value ϕ_s). Given a defined $D_n(\kappa)$ law, a set of ordinary differential equations define the DSD steady-state detonation front shape and axial velocity for the four PBX 9012 unconfined rate stick geometry diameter effect tests described in §2. The optimization of the parameters to fit the DSD model (8) to the PBX 9012 rate stick detonation front shapes and axial velocities were obtained by minimization of a merit function incorporating the differences in phase velocities and front shapes between the DSD calculations and experimental data. The details of the calibration process are described in [17], with the specific error minimization merit function used given in [5]. This methodology produces the DSD model parameters shown in Table 3, while the comparison of the DSD model calculations to experimental data, after calibration to the data, appears in Fig. 10. The DSD model fit captures the axial velocity and front shape data well, with a RMS error level of 6.1 m/s and 13.5 μm, respectively, across all four tests.

Figure 11a shows the D_n variation with κ for the calibrated PBX 9012 DSD propagation law, along with a prior result for PBX 9501 [17]. The overall trend between PBX 9012 and PBX 9501 is similar, except for a change in concavity for the PBX 9012 variation at higher propagation speeds. This turn up is reminiscent of the $D_n(\kappa)$ response seen for PBX 9502 [7] near D_{CJ}, where the turn up corresponds to the presence of a slow reaction stage due to carbon coagulation behind the main reaction layer. For the insensitive HE PBX 9502 (95 wt% TATB (2,4,6-triamino-1,3,5-trinitrobenzene)/5 wt% Kel-F 800 (poly(chlorotrifluoroethylene-co-vinylidene fluoride))), the effects of the slow reaction stage are detected in the large diameter experimental tests, and similarly for PBX 9012, the turn up is strongly influenced by the fitting of the large diameter (50.7 mm) front shape. That said, due to the relatively small number of tests, we cannot definitely attribute the turn up to a secondary reaction stage, but merely note the similarity with PBX 9502. However, if it is caused by secondary reaction, the effect is a lot weaker than that seen for PBX 9502. Returning to Fig. 11a, the offset in normal speed D_n at any given κ between the PBX 9012 and PBX 9501 $D_n(\kappa)$ functions remains within 200 m/s throughout the shown range. Scaling each curve by its individual D_{CJ} value gives the comparison in Fig. 11b. The PBX 9012 result is close to the PBX 9501 result, with differences remaining within 0.5% relative to the PBX 9501 curve for the shown range.

4.1.2. Pseudo-reaction-zone energy release model

The PRZ energy release model was developed [24, 26–29] to capture the effect of the finite-length reaction zones in real detonations, within the context of a PB model. The energy addition into the flow is achieved via a spatially-distributed, finite rate of reaction, in a similar manner to reactive burn (RB) models for detonation propagation. Previously, PB methods considered the reaction zone as a vanishingly thin layer, negating the potentially significant influence of

the spatially-distributed reaction zone on the evolution of the product material [21]. For PBX 9012, we assume a single stage reaction, with the PRZ model reaction rate (Λ) depending on the reaction progress ($\lambda \in [0, 1]$), the time-of-arrival field of the detonation at any point in the HE geometry (t_b) evaluated from the DSD model, and the DSD front normal detonation velocity (D_{ns}) at the point of wave arrival. Specifically,

$$\Lambda = \Lambda(\lambda, D_{ns}, t_b) = H(t - t_b)k_1(1 - \lambda)^{\nu_1}\left(\frac{D_{ns}}{D_{CJ}}\right)^{N_1}, \tag{9}$$

where k_1, ν_1 and N_1 are reaction kinetic parameters and H is the Heaviside function which activates Λ only for $t > t_b$.

For the reactant and product EOSs needed by the PBX 9012 PRZ model, we use the EOS form developed by Davis *et al.* [30, 31] in the form presented in [25]. The internal energy for the reactants is given by $e_R(p_R, v_R)$ and that for the products by $e_P(p_P, v_P)$ for pressure p and specific volume v. The subscripts $\{~\}_R$ and $\{~\}_P$ represent the reactant and product state, respectively. The mixture internal energy e and specific volume v are given by

$$e = (1 - \lambda)e_R(p_R, v_R) + \lambda e_P(p_P, v_P), \tag{10}$$
$$v = (1 - \lambda)v_R + \lambda v_P. \tag{11}$$

As in RB methods, the PRZ model requires a thermodynamic closure to complete the definition of the mixture in the RZ. For our purposes, we assume pressure equilibrium, $p_P = p_R$, and volume equality $v_R = v_P$ as used in [32]. Equations (9)–(11) are then combined with the flow equations,

$$\frac{D\rho}{Dt} + \rho\nabla \cdot \mathbf{u} = 0, \quad \frac{D\mathbf{u}}{Dt} = -\frac{1}{\rho}\nabla p,$$
$$\frac{De}{Dt} = \frac{p}{\rho^2}\frac{D\rho}{Dt}, \quad \frac{D\lambda}{Dt} = \Lambda, \tag{12}$$

to complete the specification of the DSD/PRZ programmed burn model for PBX 9012. Here ρ ($= 1/v$) is the density, while $\mathbf{u}$ is the flow velocity and D/Dt is the total derivative.

Davis Reactants EOS for PBX 9012. The Davis internal energy form for reactants is given by

$$e_R(p_R, v_R) = e_R^s(v_R) + \frac{v}{\Gamma_R(v_R)}(p_R - p_R^s(v_R)), \tag{13}$$

where the reference isentrope functions $e_R^s(v_R)$ and $p_R^s(v_R)$ and Grüneisen gamma $\Gamma_R(v_R)$ are defined by

$$\Gamma_R(v_R) = \begin{cases} \Gamma_R^0 + Zy, v_R \leq v_0 \\ \Gamma_R^0, v_R > v_0 \end{cases} \tag{14}$$

$$p_R^s(v_R) = \begin{cases} \hat{p}\left[C\dfrac{(4By)^4}{4!} + \dfrac{y^2}{(1-y)^4} + \displaystyle\sum_{j=1}^{3}\dfrac{(4By)^j}{j!}\right], \\ \hfill v_R \leq v_0 \\ \hat{p}(\exp(4By) - 1), v_R > v_0 \end{cases} \tag{15}$$

$$e_R^s(v_R) = \begin{cases} \frac{1}{\rho_0}\int_0^y p_R^s(y')dy', v_R \leq v_0 \\ \frac{\hat{p}}{4B\rho_0}(\exp(4By) - 1 - 4By), v_R > v_0 \end{cases} \tag{16}$$

14
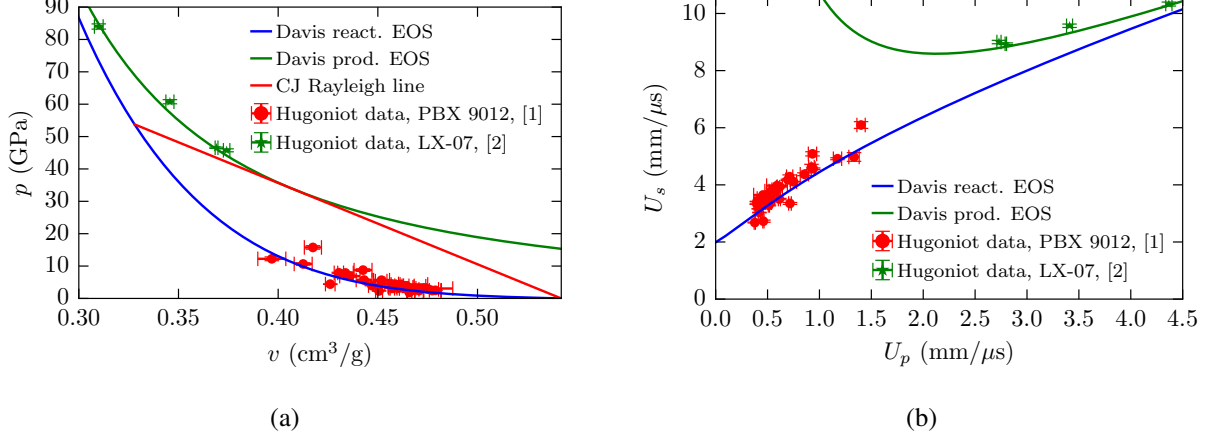
Figure 12: PBX 9012 reactants and products Hugoniot data and results from the Davis EOS model fits in both the $p - v$, (a), and shock velocity (U_s) - particle speed (U_p), (b), Hugoniot planes.

	Davis reactants EOS			Davis products EOS			Reaction rates		
							PRZ PB model		
						$k_1 =$	206.8911	μs^{-1}	
$A =$	1.9900	mm/μs	$a =$	0.9132		$\nu_1 =$	0.51248		
$B =$	2.2000		$b =$	0.7317		$N_1 =$	1.38477		
$C =$	6.5000		$n =$	2.2010			Modified WSD RB model		
$\Gamma_R^0 =$	0.6185		$k =$	1.3820		$k_{IG} =$	0.0035161	μs^{-1} GPa$^{-n_{IG}}$	
$Z =$	0.0		$v_c =$	0.9586	cm^3/g	$n_{IG} =$	2.86064		
$\rho_0 =$	1.845	g/cm^3	$p_c =$	1.4325	GPa	$\rho_c =$	2.25760	g/cm^3	
$T_0 =$	293.0	K	$E_{det} =$	5.664	kJ/g	$k_{DG} =$	0.0038243	μs^{-1} GPa$^{-n_{DG}}$	
						$n_{DG} =$	3.00426		
						$c =$	0.78971		

Table 4: Calibrated model parameters for PBX 9012. The CJ velocity is 8.590 mm/μs and the CJ pressure and density are respectively 33.78 GPa and 2.45 g/cm^3. Using the Chapman-Jouguet velocity, the resulting von Neumann state pressure and density are 53.77 GPa and 3.05 g/cm^3, respectively.

where

$$y = 1 - v_R/v_0, \quad \hat{p} = \rho_0 A^2/4B. \tag{17}$$

Here, A, B, C, Γ_R^0, and Z parameterize the Davis reactant EOS, with ρ_0 ($= 1/v_0$) the initial reactant density. The EOS parameters have been recalibrated by fitting to a series of PBX 9012 reactant Hugoniot data experiments [4] using the model calibration strategy outlined in [4]. The derived parameters are shown in Table 4. The PBX 9012 reactants EOS Hugoniot data and model fits are shown in Fig. 12.

Davis products EOS for PBX 9012. The Davis internal energy form for products is given by

$$e_P(p_P, v_P) = e_P^s(v_P) + \frac{v_P}{\Gamma_P(v_P)}(p_P - p_P^s(v_P)), \tag{18}$$

15

where the reference isentrope functions $e_P^s(v_P)$ and $p_P^s(v_P)$ and Grüneisen gamma $\Gamma_P(v_P)$ are defined by

$$p_P^s(v_P) = p_c \frac{\left[\frac{1}{2}(v_P/v_c)^n + \frac{1}{2}(v_P/v_c)^{-n}\right]^{a/n}}{(v_P/v_c)^{k+a}} \times$$
$$\left[\frac{k-1+F(v_P)}{k-1+a}\right] \tag{19}$$

$$e_P^s(v_P) = e_c \frac{\left[\frac{1}{2}(v_P/v_c)^n + \frac{1}{2}(v_P/v_c)^{-n}\right]^{a/n}}{(v_P/v_c)^{k-1+a}} - E_{det}, \tag{20}$$

$$\Gamma_p(v_P) = k - 1 + (1-b)F(v_P), \tag{21}$$

where

$$F(v_P) = \frac{2a(v_P/v_c)^{-n}}{(v_P/v_c)^n + (v_P/v_c)^{-n}}, \quad e_c = \frac{p_c v_c}{k-1+a}. \tag{22}$$

Here, p_c, v_c, a, k, n, b and E_{det} parameterize the Davis product EOS. We use a new hydrocode-based calibration methodology that simultaneously calibrates the products EOS parameters and the PRZ model rate parameters k_1, ν_1 and N_1 defined in (9). The motivation for this process is that the finite length of the reaction zone has some effect on the CYLEX test wall motion, and therefore must influence the calibration of the product EOS obtained from the CYLEX tests. A detailed description of the new methodology will be presented in a future publication. Below, we describe the essential elements that enable the product EOS and PRZ model parameters for PBX 9012 to be obtained.

Davis products EOS and reaction rate calibration. The process begins by calibrating an initial PBX 9012 Davis product EOS parameter set through a traditional programmed burn approach as described in [5] (see also Appendix A). Given this initial EOS parameter set, the PRZ rate model parameters in (9) are calibrated according to the procedure described in [24]. Essentially, the latter process is designed to ensure that the rate of energy release in the PRZ reaction stage is synchronized to the DSD surface motion. This is achieved by iterating on the PRZ rate parameters until the diameter effect and corresponding front shapes obtained from the PRZ model for the unconfined rate stick charge sizes in §2 closely match those of the corresponding DSD calculations (§4.1.1). A merit function error minimization technique is used to determine the match criteria [24]. The next step is to use this newly calibrated PRZ reaction rate model to generate a new Davis product EOS parameterization. This is by achieved by using the DSD/PRZ programmed burn model in a Lagrangian hydrocode (FLAG) simulation [5] to generate a prediction of the wall motion from the PBX 9012 CYLEX test described in §2, and iterating on the product EOS parameters until the hydrocode-calculated wall motion closely matches the experimentally determined wall motion. Again, a merit function error minimization technique is used to determine the match criteria for the wall motion. With the change in products EOS parameters, we then recalibrate the PRZ reaction rate parameters as described above, and continue the cycle until the PRZ rate and product EOS parameters have converged. Effectively, this amounts to a successive approximation iteration technique. As noted above, the technical details of the iterative process will be described in a future publication.

16
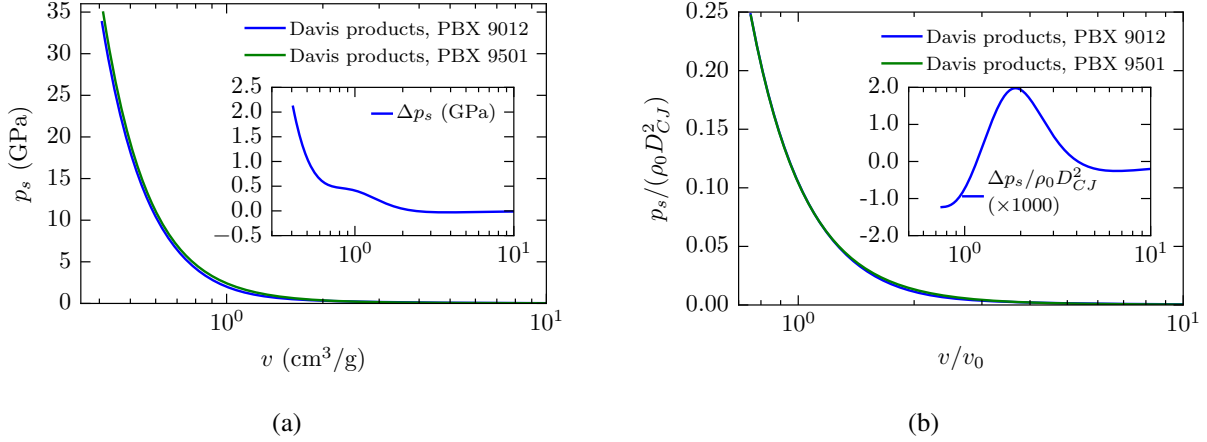
Figure 13: (a) The calibrated Davis products form resulting from the hydrocode-based PRZ calibration process. An equivalent result for PBX 9501 [29] also appears. (b) The same comparison is made as in (a) but for the $\rho_0 D_{CJ}^2$-scaled dimensionless pressure. In both subfigures, the inset quantifies the fine differences between the curves.

The calibrated parameters for the Davis products EOS and PRZ reaction rate for PBX 9012 obtained through the above process appear in Table 4. The PBX 9012 product Hugoniot is shown in Fig. 12 along with previously obtained overdriven products state data [2] for the closely related HE LX-07. Although not calibrated to the overdriven Hugoniot data for LX-07, the DSD/PRZ model CYLEX-test derived PBX 9012 products EOS gives a good prediction of the LX-07 data. The PBX 9012 Davis products CJ isentrope is shown in Fig. 13a (along with an equivalent result for PBX 9501 [29]). The shape of the products isentrope is important as it largely establishes the work done on surrounding (metal or other) confinement materials during detonation propagation. The CJ state, the highest point in each curve, and the isentrope energy $\int_{v_{CJ}}^{\infty} p_P^s(v_P) \, dv_P$ are larger for PBX 9501. However, Fig. 13b compares the PBX 9012 and PBX 9501 isentropes on scaled pressure (with $\rho_0 D_{CJ}^2$) and volume (with v_0) axes. The two curves largely collapse together and thus demonstrate a scaling similarity between the PBX 9012 and PBX 9501 pressure isentrope variations. The insets within each subfigure in Fig. 13 quantify the closeness of the isentrope curves. This observation suggests that it may be possible to predict the product pressure isentrope for an HMX-based target HE using measurable properties for the target HE, together with a simple scaling of a previously determined HMX-based HE product isentrope. The PBX 9012 CYLEX wall motion derived from the PBX 9012 DSD/PRZ model is shown in Fig. 14, showing that the DSD/PRZ model has been calibrated to reproduce the wall motion from the experimental data to within the probe-to-probe variation of that data.

4.2. Modified WSD RB model for PBX 9012

We now calibrate a reactive burn model for detonation performance of PBX 9012, again based on the experimental data in §2. Our RB model choice is a modification of the Wescott-Stewart-Davis (WSD) model [25]. The PBX 9012 reactant and product EOSs are directly imported from the calibrated Davis EOSs in §4.1.2. We employ a slightly modified reaction rate form to the original WSD model [25] given by

$$\Lambda(\rho, p, \lambda, \rho_s) = r_{IG} W + r_{DG}(1 - W). \tag{23}$$

17
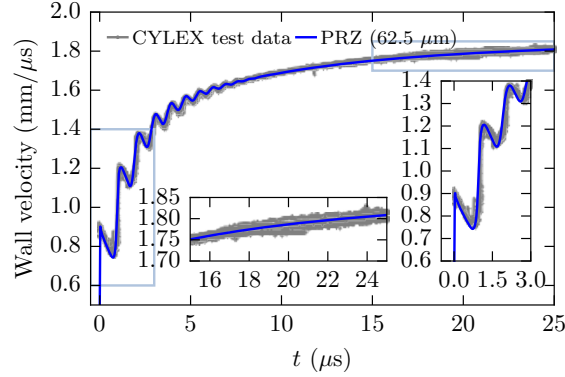
Figure 14: Comparison of the calibrated PRZ calculation to the CYLEX test derived wall motion. Insets show zoomed-in regions of the evolution (outline in light blue rectangles in the larger figure).

It consists of two sequential components representing ignition growth (r_{IG}) and detonation growth (r_{DG}) phases, and where W is a smooth blending function. The functional dependencies are

$$r_{IG} = k_{IG}(1 - \lambda)^c p^{n_{IG}}, \ r_{DG} = k_{DG}(1 - \lambda)^c p^{n_{DG}}, \tag{24}$$

$$W = \frac{1}{2}\left(1 - \tanh\left(50\left(\frac{\rho_s}{\rho_c} - 1\right)\right)\right). \tag{25}$$

Thus, the reaction rate Λ depends on the pressure (p), density (ρ), density immediately behind the lead shock (ρ_s) and reaction progress (λ) and on a number of rate parameters. These are, for the initiation stage, k_{IG}, n_{IG} and ρ_c and for the detonation propagation stage, k_{DG}, c, and n_{DG}. The calibration of these parameters is split into sequential propagation and initiation steps, as described below. As in [5, 32, 33] and in the PRZ model calibration (§4.1.2), we also assumed pressure equilibrium and specific volume equality to close the modified WSD RB model. Related modifications to the WSD reaction rate and closure model have previously been shown to accurately reproduce the dynamics of detonation propagation in 2D circular arc validation experiments for both the conventional HE PBX 9501 and the insensitive HE PBX 9502 [32, 33]. Given that the EOSs for the WSD model are imported from the PRZ model calibration (§4.1.2), we need only to calibrate the reaction rate parameters to complete the specification of the modified WSD model for PBX 9012.

4.2.1. Propagation rate terms

The propagation stage rate parameters k_{DG}, c, and n_{DG} are calibrated to the unconfined rate stick tests in §3.1, i.e. the same experimental data used for the DSD model calibration in §4.1.1. The shock-attached computational framework we use to determine the steady rate stick geometry phase velocities and front shapes for the modified reactive burn WSD model needed for the calibration process is described in [5, 32, 33]. The rate stick simulations use 1.875 μm uniform mesh spacing (except for the largest rate stick which uses 3.75 μm). The optimized propagation stage rate parameter set appears in Table 4, while the fitted unconfined rate stick

18
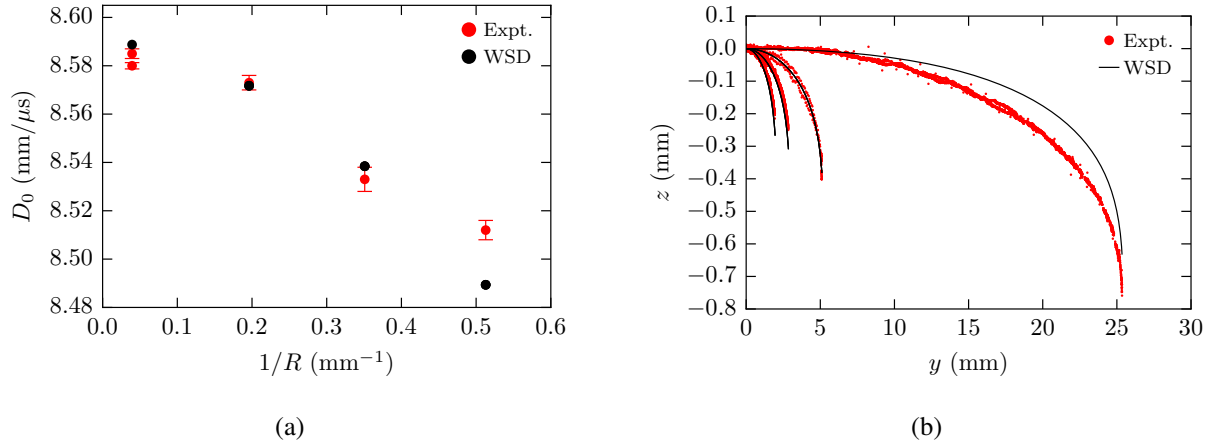
Figure 15: (a) Diameter effect and (b) detonation shock shape calculations from the PBX 9012 fitted, modified WSD model compared to the experimental data.

(a) Shot no. 2s-1101

(b) Shot no. 1s-1673
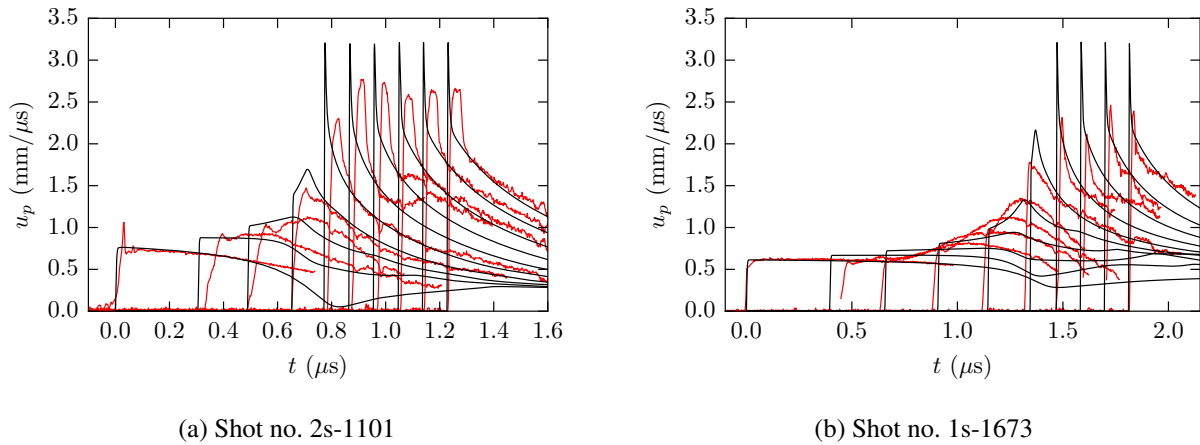
Figure 16: Comparison of embedded gauge results for the fitted, modified WSD model and the gas-gun impact experiments 2s-1101 and 1s-1673 from Burns and Chiquete [4]. The simulations are the black lines, while the experiments are shown in red.

calculations are compared to the experimental data in Fig. 15. The calibration process employed the numerical minimization of an error functional that separately incorporates phase velocity and front shape errors with weight factors to balance the contribution of each into the global error metric. The results show that the calculated phase velocities are mostly within the standard error of each measurement, except for the smallest rate stick. The fit error for the largest rate stick front shapes was noticeably larger as well in relation to the smaller rate sticks. Overall, the fit quality is acceptable especially for the higher range in charge-diameters.
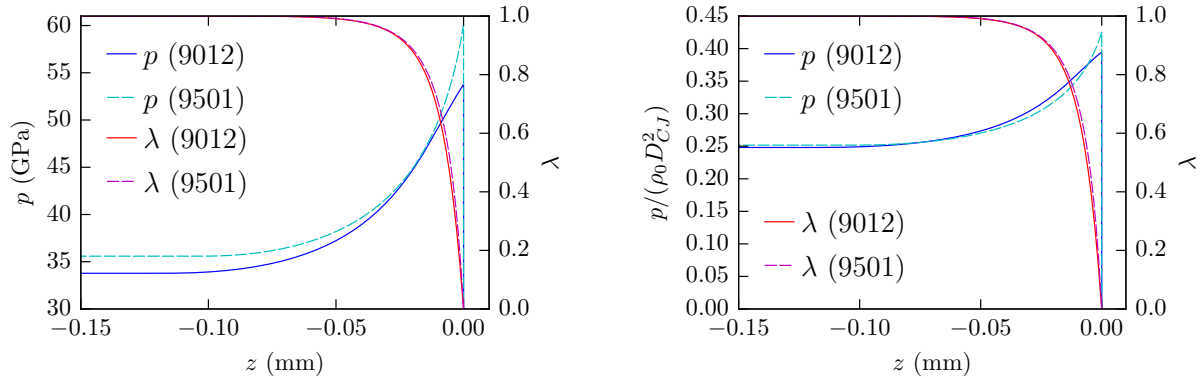
Figure 17: (a) The 1D steady-state CJ wave structure both for the calibrated PBX 9012 model and for a counterpart for PBX 9501 [32]. (b) As in (a) with the pressure profiles scaled with $\rho_0 D_{CJ}^2$.

4.2.2. Initiation rate terms

The initiation stage reaction rate parameters for PBX 9012 were calibrated based on the shock initiation data reported in Burns and Chiquete [4]. The initiation rate calibration computations were performed using a multi-material numerical methodology described in [34–36] and require the simulation of 1D plate impact experiments performed at the various projectile speeds utilized in the gas-gun embedded gauge experiments. The mesh resolution employed in the multi-material calibration simulations was 6.25 μm. The calibration error metric uses data from both a tracing diagnostic for the shock path and the embedded Lagrangian gauge profiles for the particle velocity. After minimization, the optimized parameters for the modified WSD initiation rate are shown in Table 4. A selection of shock-to-detonation calculations for the higher pressure impacts are shown in Fig. 16 (emphasizing the especially good correspondence at higher input pressures). This completes the specification of the modified WSD reactive burn model for PBX 9012.

4.2.3. ZND profile

Figure 17 shows the corresponding structure of the 1D Zeldovich-von Neumann-Döring (ZND) model for the PBX 9012 detonation model. It has a total reaction zone length of around 110 μm, comparable though longer than the scale found for PBX 9501 [32], which showed a total reaction zone length scale of $\approx$ 100 μm. A comparison of the PBX 9012 and PBX 9501 ZND profiles is also made in Fig. 17a. The 50% reaction progress length scales are given by 5.2 μm and 6.1 μm for PBX 9501 and PBX 9012, respectively. The spatial pressures are different, primarily as the von Neumann and CJ pressures are higher for PBX 9501 than PBX 9012. However, the rate of reaction progress between the two explosives is similar (Fig. 17a). This again suggests a scaling relation between the explosives with different binder weight percentages. Figure 17b scales the ZND pressure profiles by $\rho_0 D_{CJ}^2$ for each explosive, revealing a reasonable overlap. When combined with the previous scaling results for PBX 9012 and PBX 9501 detonation properties, including the diameter effect (Fig. 6), CYLEX test wall motion (Fig. 8), weight percentage of HMX (Fig. 9), and the $D_n(\kappa)$ variation (Fig. 11b), this would suggest that when the hydrodynamic variables are scaled using ρ_0 and D_{CJ} for each explosive, the rate of reaction,

(a) $d = 5.7$ mm (b) $d = 3.9$ mm
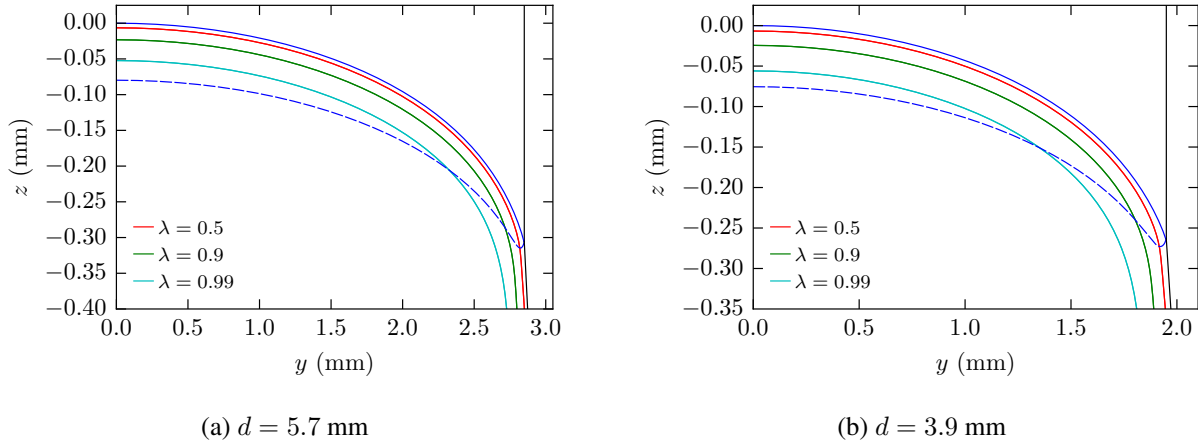
Figure 18: The 2D steady-state detonation reaction zone structure for two different PBX 9012 rate stick geometry charge diameters. The region bounded by the detonation front (blue line) and the sonic locus (dashed blue line) is known as the detonation driving zone (or DDZ). Reaction progress contours are also plotted at 0.5, 0.9, and 0.99 completion and denoted by the red, green and cyan lines, respectively. The black lines are the edge of the HE domain (note that this boundary is deflected intersection with the detonation shock).

and thus perhaps the overall kinetic mechanisms, for PBX 9012 and PBX 9501 are similar.

4.2.4. Detonation driving zone (DDZ) structure for PBX 9012

The 2D steady-state rate stick detonation wave structure for the calibrated PBX 9012 WSD model is illustrated in Fig. 18 for two unconfined charge diameters of 5.7 mm and 3.9 mm. Each plot contains the detonation driving zone (DDZ) structure, i.e. the region of the flow bounded by the shock front and the sonic locus (relative to the steady traveling axial speed of the shock). The axial propagation of the wave is supported by the energy release that occurs in the DDZ, although information from the material interfaces, or Prandtl-Meyer fan at the intersection of the detonation shock and material interface, can propagate through the supersonic regions of the flow and influence the DDZ shape [37, 38]. Several reaction progress contour lines reveal how the energy release is spatially distributed in the reaction zone, and show weakened reaction near the edge, typical of 2D steady-state detonation [21]. For both diameters, near the charge centerline, the sonic locus remains close to the point of reaction completion. The overall scale of the DDZ on the centerline is 70-80 μm for these PBX 9012 diameters. As the diameter drops from 5.7 mm to 3.9 mm, the DDZ sonic locus enters the main reaction layer at an earlier relative stage, reducing the amount of the energy release in the DDZ, and resulting in a lowering of the axial propagation speed [21, 39]. Figure 18 reinforces the fine spatial scales associated with the 2D DDZ regions for PBX 9012 detonation.

5. Summary

A series of detonation performance experiments are described for PBX 9012, an HMX-based high explosive (HE) intended for booster applications. The generated data is compared to equivalent data for PBX 9501, another HMX-based HE that is significantly more energetic and well-characterized in the condensed-phase HE literature. The comparison reveals a novel scaling

21

relation for PBX 9012's diameter effect and cylinder expansion test wall velocity profile. These measured properties are well described as scaled down versions of PBX 9501 equivalents (via the ratio of CJ speeds for the two explosives). The ratio can be accurately predicted via consideration of the HMX mass ratio between the explosives. Furthermore, an investigation of archival literature revealed that the ratio of the square of the detonation velocity and HMX mass ratios scales nearly linearly for a variety of formulations spanning significant differences in HMX content and pressing densities.

Based on these scaling relationships, we hypothesized that the reduced HMX content causes a systemic offset in the energy available for propagation for a variety of unconfined charge diameters and in the HE's ability to work on surrounding materials. The calibration of detonation performance models for PBX 9012 was then leveraged to provide more quantitative evidence for these hypotheses. For the energy release, the offset is reflected in the calibrated products pressure isentrope which largely sets the trajectory of the wall motion in a CYLEX test simulation. A comparison to a prior result for PBX 9501 shows that the isentrope variation is nearly coincident on a normalized pressure axis. On the propagation, because the diameter effect for a given explosive depends on the the energy release distribution in the HE's reaction zone and its interaction with flow divergence (as mediated by the specific charge-size), the proportionally similar results for the two explosives indicate that the energy release in the RZ must also be similarly structured. This is reflected in the reactive burn modeling of the explosives, which allows comparisons of the resulting reaction zone profiles and the reaction rate laws. The energy release profile is found to be spatially similar between the explosives, even though significant differences exist in their pressure profiles. We also confirm that the kinetics of the two explosives are similar as revealed by the parameters of the pressure-sensitive rate law that defines the Wescott-Stewart-Davis model. This is in spite of the significant drop in PBX 9012's HMX content, reduced strength post-shock flow conditions and differences in binder material and pressing density. The scaling relations found in this work offer a method to predict important detonation performance properties for compositionally related explosives that contain inert or weakly energetic binders. The quality of these predictions will be assessed for other explosive pairs in future work.

References

[1] B. M. Dobratz, P. C. Crawford, LLNL Handbook of Explosives, Tech. Rep. UCRL-52997 Rev2, Lawrence Livermore National Laboratory, 1985.

[2] L. G. Green, E. L. Lee, A. R. Mitchell, C. M. Tarver, Supra-compression of LX-07, LX-17, PBX 9404, and RX-26-AF and the equations of state of the detonation products, in: Proceedings of the 8th International Detonation Symposium, Office of Naval Research, 587–595, 1985.

[3] L. G. Green, R. J. Wasley, P. E. Kramer, Shock initiation of LX-07-2 and LX-10-0, Tech. Rep. UCRL-50851, Lawrence Livermore National Laboratory, 1970.

[4] M. J. Burns, C. Chiquete, Shock initiation of the HMX-based explosive PBX 9012: Experiments, uncertainty analysis, and unreacted equation-of-state, J. Appl. Phys. 127 (2020) 215107.

[5] C. Chiquete, S. I. Jackson, E. K. Anderson, M. Short, Detonation performance experiments and modeling for the DAAF-based high explosive PBX 9701, Combust. Flame 223 (2020) 382–397, doi: https://doi.org/10.1016/j.combustflame.2020.10.009.

[6] C. Chiquete, S. I. Jackson, Detonation performance of the CL-20-based explosive LX-19, Proc. Combust. Instit. 38 (2020), doi:https://doi.org/10.1016/j.proci.2020.07.089.

[7] S. I. Jackson, M. Short, Scaling of detonation velocity in cylinder and slab geometries for ideal, insensitive and non-ideal explosives, J. Fluid Mech. 773 (2015) 224–266.

[8] S. I. Jackson, Scaling of the detonation product state with reactant kinetic energy, Combust. Flame 190 (2018) 240–251.

[9] C. A. Handley, B. D., Lambourn, N. J. Whitworth, H. R. James, W. J. Belfield, Understanding the shock and detonation response of high explosives at the continuum and meso scales, Appl. Phys. Rev. 5 (2018) 011303.

[10] E. K. Anderson, C. Chiquete, S. I. Jackson, Experimental measurement of energy release from an initiating layer in an insensitive explosive, Proc. Combust. Inst. doi:https://doi.org/10.1016/j.proci.2020.07.150.

[11] T. R. Gibbs, A. Popolato, LASL Explosive Property Data, University of California Press, 1980.

[12] S. I. Jackson, An analytic method for two-dimensional wall motion and product isentrope from the detonation cylinder test, Proc. Combust. Inst. 35 (2) (2015) 1997–2004.

[13] S. I. Jackson, Scaled cylinder test experiments with insensitive PBX 9502 explosive, in: Proceedings of the 15th International Detonation Symposium, Office of Naval Research, 171–180, 2015.

[14] S. I. Jackson, The dependence of Ammonium-Nitrate Fuel-Oil (ANFO) detonation on confinement, Proc. Combust. Instit. 36 (2017) 2791–2798.

[15] R. Engelke, J. B. Bdzil, A study of the steady-state reaction-zone structure of a homogeneous and a heterogeneous explosive, Phys. Fluids 26 (1983) 1210–1221.

[16] W. C. Davis, T. R. Salyer, S. I. Jackson, T. Aslam, Explosive-driven shock waves in argon, in: Proceedings of the 13th International Detonation Symposium, Office of Naval Research, 1035–1044, 2006.

[17] C. Chiquete, M. Short, E. K. Anderson, S. I. Jackson, Detonation shock dynamics modeling and calibration of the HMX-based conventional high explosive PBX 9501 with application to the two-dimensional circular arc geometry, Combust. Flame 222 (2020) 213–232.

[18] M. A. Zocher, T. D. Aslam, S. I. Jackson, E. K. Anderson, Numerical modeling comparing slab to cylinder test expansion geometries for PBX 9501, in: Proceedings of the 16th International Detonation Symposium, Office of Naval Research, 1137–1147, 2018.

[19] A. Edgar, J. Yang, M. Chavez, M. Yang, D. Yang, Physical characterization of Bis (2, 2-dinitropropyl) acetal and Bis (2, 2-dinitropropyl) formal, J. Ener. Mats. 38 (2020) 483–503.

[20] J. B. Bdzil, D. S. Stewart, The dynamics of detonation in explosive systems, Annu. Rev. Fluid Mech. 39 (2007) 263–292.

[21] M. Short, J. J. Quirk, High explosive detonation-confiner interactions, Annu. Rev. Fluid Mech. 50 (2018) 215–242.

[22] J. B. Bdzil, D. S. Stewart, Modeling two-dimensional detonations with detonation shock dynamics, Phys. Fluids A: Fluid Dyn. 1 (1989) 1261–1267.

[23] J. B. Bdzil, W. Fickett, D. S. Stewart, Detonation shock dynamics: a new approach to modeling multi-dimensional detonation waves, in: Proceedings of the 9th International Detonation Symposium, Office of Naval Research, 730–742, 1989.

[24] C. Chiquete, M. Short, C. D. Meyer, J. J. Quirk, Calibration of the Pseudo-Reaction-Zone model for detonation wave propagation, Combust. Theory Modell. (2018) 744–776.

[25] B. L. Wescott, D. S. Stewart, W. C. Davis, Equation of state and reaction rate for condensed-phase explosives, J. Appl. Phys. 98 (2005) 053514.

[26] T. N. Dey, M. S. Shaw, A coupled pseudo-reaction zone and products EOS model for PBX 9502, Tech. Rep. LA-UR-05-7511, Los Alamos National Laboratory, 2005.

[27] B. L. Wescott, Development of a generalized Pseudo-Reaction Zone model for non-ideal explosives and application to ANFO, Tech. Rep. LA-UR-06-8661, Los Alamos National Laboratory, 2006.

[28] B. L. Wescott, Generalized Pseudo-Reaction Zone model for non-ideal explosives, in: AIP conference proceedings, vol. 955, American Institute of Physics, 433–436, 2007.

[29] C. Chiquete, M. Short, DSD/Pseudo-Reaction Zone model for high explosive detonation simulation: Flag user guide, Tech. Rep., Los Alamos National Laboratory, U.S.A., 2020.

[30] W. C. Davis, Complete equation of state for unreacted solid explosive, Combust. Flame 120 (3) (2000) 399–403.

[31] D. S. Stewart, S. Yoo, W. C. Davis, Equation of state for modeling the detonation reaction zone, in: Proceedings of the 12th International Detonation Symposium, Office of Naval Research, 1–11, 2002.

[32] M. Short, E. K. Anderson, C. Chiquete, S. I. Jackson, Experimental and modeling analysis of detonation in circular arcs of the conventional high explosive PBX 9501, Proc. Combust. Instit. 38 (2020), doi: https://doi.org/10.1016/j.proci.2020.07.107.

[33] M. Short, C. Chiquete, J. B. Bdzil, J. J. Quirk, Detonation diffraction in a circular arc geometry of the insensitive high explosive PBX 9502, Combust. Flame (2018) 1–33.

[34] J. J. Quirk, amr_sol::multimat, Tech. Rep. LA-UR-07-0539, Los Alamos National Laboratory, U.S.A., 2007.

[35] J. J. Quirk, *Amrita* - A Computational Facility (for CFD modelling), in: H. Deconinck (Ed.), 29th Computational Fluid Dynamics, von Karman Institute, 1998.

[36] J. J. Quirk, Amr_sol: Design Principles and Practice, in: H. Deconinck (Ed.), 29th Computational Fluid Dynamics, von Karman Institute, 1998.

[37] C. Chiquete, M. Short, Characteristic path analysis of confinement influence on steady two-dimensional detonation propagation, J. Fluid Mech. 863 (2019) 789–816.

[38] M. Short, C. Chiquete, J. J. Quirk, Detonation propagation for shock-driven, subsonic and supersonic confiner flow, J. Fluid Mech. 885 (2020) A17, 1–17.

[39] M. Short, J. J. Quirk, C. Chiquete, C. D. Meyer, Detonation propagation in a circular arc: reactive burn modelling,

Appendix A. Jones-Wilkins-Lee (JWL) EOSs for PBX 9012

A	B	R_1	R_2	C	ω	E_{det}	ρ_0
(GPa)	(GPa)			(GPa)		(kJ/g)	(g/cm^3)
776.513	16.448	4.520	1.370	1.382	0.3043	5.848	1.845

Table A.5: Calibrated JWL product EOS parameters for PBX 9012. The CJ detonation velocity is 8.590 mm/μs, while the CJ pressure is 35.54 GPa and the CJ specific volume is 0.4005 cm^3/g.

Products. Standard programmed burn methods typically use the Jones-Wilkins-Lee (JWL) EOS for detonation products [5]. This EOS form is given by

$$
\begin{aligned}
p(v, e) = \ & A\left(1 - \frac{\omega v_0}{R_1 v}\right)\exp\left(-\frac{R_1 v}{v_0}\right) \\
& + B\left(1 - \frac{\omega v_0}{R_2 v}\right)\exp\left(-\frac{R_2 v}{v_0}\right) \\
& + \frac{\omega}{v}(e + \lambda E_{det}),
\end{aligned}
\tag{A.1}
$$

where λ refers to the pre-programmed reaction progress (activated upon the calculated time of arrival field), E_{det} is the detonation energy, $v_0 = 1/\rho_0$, and A, R_1, R_2, B, ω are the JWL EOS parameters. The reference curve used in (A.1) is the CJ isentrope given by

$$
p_s(v) = A\exp\left(-\frac{R_1 v}{v_0}\right) + B\exp\left(-\frac{R_2 v}{v_0}\right) + C\left(\frac{v}{v_0}\right)^{-1-\omega},
\tag{A.2}
$$

where the isentrope label parameter C is defined such that $p_s(v_{CJ}) = p_{CJ}$ (see Table A.5). The JWL EOS parameters shown in Table A.5 were calibrated to the PBX 9012 CYLEX data (§2) using the hydrocode simulation-based velocity-adjusted JWL (VAJWL) methodology, as described in [5, 6]. Figure A.19 shows the fit to the Cu wall motion from the PB-based simulation of the calibrated JWL EOS compared to the experimental CYLEX data (§2). The fit is excellent.

A	B	R_1	R_2	C	ω	ρ_0
(GPa)	(GPa)			(GPa)		(g/cm^3)
60338.658	-4.498	11.471	1.177	0.757	0.842	1.845

Table A.6: Calibrated JWL EOS parameters for PBX 9502 reactants. The reference state for the isentrope label C is the ambient state.

Reactants. The JWL equation of state can also be used to represent the HE reactants in addition to the products by putting $E_{det} = 0$ in (A.1) and setting the internal energy to be zero in the ambient state. Following a calibration process similar to the Davis reactants EOS described in section 4.1.2, we derive the JWL reactants EOS parameterization given in Table A.6. The resulting JWL model Hugoniots are shown in Fig. A.20.
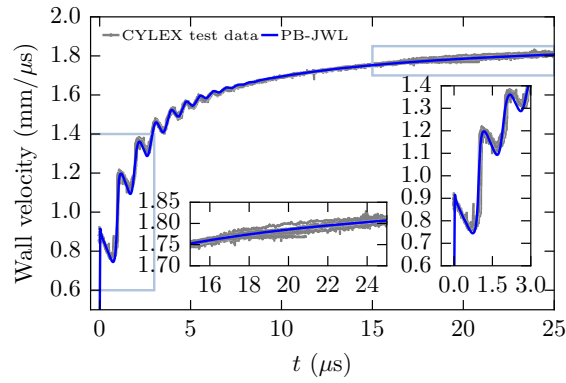
Figure A.19: CYLEX wall motion generated by the calibrated velocity-adjusted JWL PB model. Insets show detail of early and late time evolution.
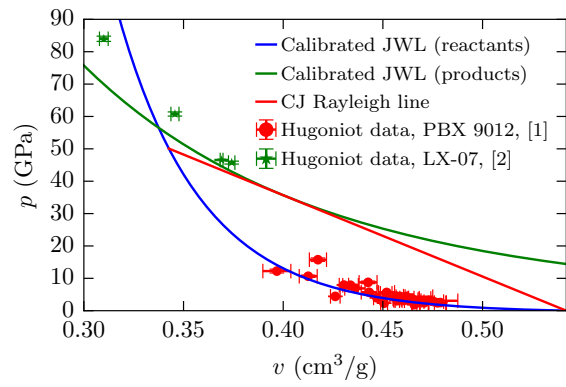
Figure A.20: The shock Hugoniot for the two JWL EOS models is compared to the PBX 9012 reactants data and the related HE LX-07 products overdriven Hugoniot data.

PBX 9012 detonation performance data supplement

Eric K. Anderson, Carlos Chiquete*, Scott I. Jackson, Ritchie I. Chicas, Mark Short

Los Alamos National Laboratory
Los Alamos, NM 87545 USA

Abstract

The detonation performance data reported in the accompanying paper is presented including pellet densities, time-of-arrival and front shape measurements from the ratestick and CYLEX tests. Additionally, the CYLEX copper wall motion obtained from the PDV probes is included.

---

1. Experimental Data Appendix

Table 1: Individual PBX 9012 pellet densities in g/cc with pellet number increasing from the detonator side. Density tolerances are $\pm$ 0.001 g/cc. Average density is reported for the 80% of the length closest to the breakout window, which spanned the D_0 measurement length.

Pellet	8-2173	8-2226	8-2169	8-2170	8-2171	8-2172
1	1.837	1.840	1.841	1.845	1.844	1.840
2	1.840	1.840	1.843	1.846	1.844	1.841
3	1.840	1.840	1.844	1.846	1.844	1.841
4	1.840	1.841	1.844	1.846	1.844	1.842
5	1.840	1.842	1.845	1.847	1.844	1.842
6	1.840	1.842	1.846	1.847	1.844	1.843
7	1.841	1.842		1.847	1.844	1.843
8	1.841	1.842		1.848	1.844	1.843
9	1.841	1.842		1.848	1.844	1.843
10	1.841	1.842		1.848	1.844	1.843
11	1.842	1.842		1.848	1.844	1.844
12	1.842	1.842		1.849	1.844	1.845
Avg.	1.841	1.842	1.844	1.847	1.844	1.843

Table 2: Individual PBX 9012 pellet diameters in mm with pellet number increasing from the detonator side. Diameter tolerances are $\pm$ 0.01 mm. Average diameter is reported for the 80% of the length closest to the breakout window, which spanned the D_0 measurement length.

Pellet	8-2173	8-2226	8-2169	8-2170	8-2171	8-2172
1	50.75	50.76	10.23	5.69	3.86	25.37
2	50.75	50.76	10.22	5.69	3.86	25.37
3	50.75	50.76	10.22	5.69	3.86	25.37
4	50.75	50.76	10.23	5.69	3.86	25.37
5	50.74	50.76	10.20	5.69	3.86	25.37
6	50.74	50.75	10.21	5.69	3.86	25.37
7	50.74	50.75		5.67	3.86	25.37
8	50.74	50.75		5.68	3.87	25.37
9	50.75	50.74		5.67	3.87	25.37
10	50.75	50.75		5.67	3.87	25.37
11	50.72	50.74		5.68	3.87	25.37
12	50.74	50.76		5.68	3.87	25.36
Avg.	50.74	50.75	10.22	5.68	3.87	25.37

Table 3: Individual and combined PBX 9012 pellet lengths in mm with pellet number increasing from the detonator side. Length tolerances are $\pm$ 0.01 mm.

Pellet	8-2173	8-2226	8-2169	8-2170	8-2171	8-2172
1	50.80	50.83	20.31	11.31	7.81	25.41
2	50.80	50.83	20.30	11.30	7.80	25.36
3	50.83	50.82	20.31	11.31	7.81	25.39
4	50.83	50.83	20.30	11.32	7.80	25.36
5	50.83	50.84	20.31	11.37	7.80	25.35
6	50.83	50.85	20.30	11.31	7.80	25.40
7	50.83	50.84		11.30	7.79	25.36
8	50.81	50.82		11.31	7.80	25.40
9	50.83	50.83		11.29	7.79	25.40
10	50.93	50.85		11.30	7.80	25.40
11	50.83	50.91		11.27	7.79	25.36
12	50.80	50.83		11.28	7.80	25.36
Total	609.95	610.08	121.83	135.67	93.59	304.55

1.1. Detonation Time of Arrival Data

8-2173 ionization data with x in mm and t in μs (22 points):

z = {0, 23.2978, 46.3115, 69.63, 92.5667, 116.036, 138.748, 161.702, 184.817, 207.797, 231.084, 254.089, 277.298, 300.5, 323.585, 347.136, 370.039, 393.036, 415.989, 439.209, 462.06, 485.388}

t = {0.3921, 3.06133, 5.70593, 8.3994, 11.067, 13.789, 16.4566, 19.0996, 21.7921, 24.4656, 27.1633, 29.8432, 32.5586, 34.9046, 37.9452, 40.6925, 43.3625, 46.0366, 48.7215, 51.4208, 54.0976, 56.8285}

8-2226 ionization data with x in mm and t in μs (22 points):

z = {0, 22.9884, 45.9158, 69.2275, 92.1575, 115.25, 138.369, 161.414, 184.468, 208.244, 231.565, 254.588, 277.53, 300.582, 323.896, 346.648, 370.005, 393.006, 416.153, 438.968, 462.084, 485.424}

t = {0.0008, 2.6413, 5.2848, 7.98533, 10.642, 13.3263, 16.0137, 18.6933, 21.3762, 24.1453, 26.8622, 29.5389, 32.2167, 34.8981, 37.6213, 40.2671, 42.9994, 45.6784, 48.3838, 51.0409, 53.7438, 56.461}

8-2169 ionization data with x in mm and t in μs (11 points):

z = {20.4616, 29.7679, 39.0562, 48.1675, 57.3093, 66.6668, 75.7927, 85.2193, 94.4619, 103.6491, 112.8134}

t = {0.26365, 1.35885, 2.4355, 3.4983, 4.56525, 5.65245, 6.71423, 7.81825, 8.89365, 9.9709, 11.0452}

8-2170 ionization data with x in mm and t in μs (11 points):

z = {11.2958, 22.6885, 33.7525, 45.1858, 56.5256, 67.7970, 79.1374, 90.4096, 101.7915, 112.9638, 124.3932}

t = {4.55987, 5.9234, 7.198, 8.5396, 9.8654, 11.1915, 12.5264, 13.8392, 15.1762, 16.4842, 17.8251}

8-2171 ionization data with x in mm and t in μs (11 points):

z = {0, 7.7455, 15.6107, 23.4199, 31.1601, 39.0687, 46.7391, 54.6944, 62.4846, 70.6097, 78.1646}

t = {4.10699, 5.01589, 5.9469, 6.85659, 7.76572, 8.7451, 9.59067, 10.5641, 11.4434, 12.4077, 13.2914}

8-2172 ionization data with x in mm and t in μs (11 points):

z = {50.7487, 73.9761, 97.1770, 120.0978, 143.3213, 166.4065, 189.6744, 212.6247, 235.8901, 258.9796, 282.0195}

t = {9.67507, 12.3556, 15.0577, 17.7284, 20.4246, 23.1228, 25.8384, 28.506, 31.232, 33.9191, 36.6079}

1.2. Detonation Front Shape Data

8-2173 front shape data in mm (75 points):

r = {-25.3282, -25.1416, -24.7283, -24.3551, -23.9552, -23.4754, -23.0088, -23.0088, -22.529, -22.0091, -21.5159, -20.7962, -20.1697, -19.3966, -18.7034, -17.8237, -17.0639, -16.3974, -15.4377, -14.6513, -13.8515, -13.0917, -12.292, -11.5988, -10.8924, -10.1326, -9.17288, -8.35978, -7.63999, -6.81357, -6.08045, -5.04075, -4.16101, -3.17463, -2.2549, -1.42847, -0.535399, 0.557615, 1.46402, 2.35709, 3.25016, 4.42315, 5.38287, 6.16931, 7.26233, 8.24871, 9.34172, 10.3947, 11.741, 12.7807, 13.9537, 15.1667, 16.1664, 17.0995, 17.9792, 18.4902, 19.01, 19.6632, 20.3696, 20.8895, 21.3693, 21.9025, 22.529, 22.9822, 23.2488, 23.5953, 23.8353, 24.1818, 24.1818, 24.5151, 24.7283, 24.9283, 25.0882, 25.2215, 25.3282}

z= {0.79309, 0.750451, 0.682228, 0.639589, 0.579894, 0.537255, 0.486088, 0.486088, 0.460504, 0.43492, 0.426393, 0.375225, 0.366698, 0.35817, 0.307003, 0.298475, 0.281419, 0.255836, 0.230252, 0.213196, 0.196141, 0.179085, 0.179085, 0.153501, 0.144973, 0.127918, 0.127918, 0.0938064, 0.102334, 0.0852785, 0.0682228, 0.0426393, 0.0426393, 0.0426393, 0.0426393, 0.0255836, 0.0341114, 0.0341114, 0.0255836, 0.0426393, 0.0255836, 0.0170557, 0.0170557, 0.0255836, 0.0170557, 0., 0.0170557, 0.0341114, 0.0426393, 0.0682228, 0.0938064, 0.0938064, 0.11939, 0.153501, 0.179085, 0.187613, 0.187613, 0.213196, 0.247308, 0.264363, 0.281419, 0.349642, 0.35817, 0.383753, 0.392281, 0.409337, 0.43492, 0.460504, 0.460504, 0.494615, 0.537255, 0.562838, 0.588422, 0.622533, 0.656645}

8-2226 front shape data in mm (257 points):

r = {-25.3518, -25.0645, -24.9523, -24.6739, -24.5213, -24.3731, -24.2609, -24.1487, -23.7805, -23.6683, -23.5067, -23.3944, -23.2822, -22.9904, -22.8782, -22.6043, -22.4921, -22.2182, -22.106, -21.9399, -21.8276, -21.6346, -21.5089, -21.3966, -21.1901, -20.9612, -20.8489, -20.6424, -20.5077, -20.3955, -20.2788, -19.9915, -19.8388, -19.6952, -19.529, -19.3764, -19.2417, -19.1025, -18.9634, -18.7075, -18.5952, -18.474, -18.2047, -18.0834, -17.8814, -17.7333, -17.6076, -17.4774, -17.3472, -17.1676, -16.9341, -16.7815, -16.5301, -16.2697, -16.1395, -15.9959, -15.8253, -15.6457, -15.511, -15.2686, -15.1518, -15.0351, -14.8915, -14.7253, -14.4694, -14.3348, -14.1731, -14.025, -13.8858, -13.7062, -13.4863, -13.3112, -13.1002, -12.9206, -12.7814, -12.6422, -12.4986, -12.3325, -12.1305, -11.9329, -11.7533, -11.5962, -11.3448, -11.2326, -11.0844, -10.9632, -10.824, -10.631, -10.4783, -10.2853, -10.1371, -10.0114, -9.74207, -9.58943, -9.41435, -9.24375, -9.0507, -8.90704, -8.77685, -8.63318, -8.41769, -8.21567, -8.01813, -7.84753, -7.70836, -7.49736, -7.31329, -7.12024, -6.99454, -6.83292, -6.6309, -6.45132, -6.33908, -6.16399, -5.92605, -5.6522, -5.49507, -5.29753, -5.07755, -4.89348, -4.73186, -4.49841, -4.35475, -4.18864, -3.97764, -3.7397, -3.57808, -3.38503, -3.14709, -2.96303, -2.69366, -2.46021, -2.2941, -2.1235, -1.9529, -1.76435, -1.54437, -1.3603, -1.13134, -0.969718, -0.772183, -0.583627, -0.354665, -0.139172, 0.152641, 0.408539, 0.601584, 0.911355, 1.18072, 1.40968, 1.66558, 1.96188, 2.23574, 2.50959, 2.66672, 2.96303, 3.20546, 3.54216, 3.73072, 4.11681, 4.4176, 4.59718, 4.87104, 5.12694, 5.49507, 5.70158, 6.04278, 6.19542, 6.375, 6.65334, 6.87333, 7.15167, 7.29084, 7.4794, 7.63653, 7.85651, 8.0316, 8.25158, 8.48952, 8.71399, 8.90704, 9.136, 9.37394, 9.60739, 9.91267, 10.0698, 10.2988, 10.4783, 10.64, 10.7971, 10.9856, 11.3134, 11.466, 11.6097, 11.7982, 12.126, 12.2562, 12.6737, 12.9026, 13.2124, 13.4189, 13.5895, 13.7871, 14.007, 14.218, 14.4021, 14.5996, 14.8286, 15.071, 15.2102, 15.4077, 15.5649, 15.7489, 15.9061, 16.0452, 16.2922, 16.4717, 16.6019, 16.8668, 17.0239, 17.1766, 17.3831, 17.6704, 17.8904, 18.1104, 18.3349, 18.5773, 18.712, 19.0891, 19.3001, 19.4213, 19.7939, 19.96, 20.1082, 20.3596, 20.5437, 20.7996, 21.0959, 21.2754, 21.4685, 21.7468, 22.0252, 22.1464, 22.2631, 22.51, 22.6312, 23.0398, 23.152, 23.4214, 23.8299, 23.9422, 24.2474, 24.3597, 24.7009, 24.9523, 25.1543, 25.2665}

z= {0.854174, 0.726474, 0.703772, 0.652691, 0.624313, 0.604449, 0.595936, 0.593098, 0.553369, 0.53918, 0.533504, 0.524991, 0.510802, 0.493775, 0.485262, 0.468235, 0.459722, 0.451208, 0.445533, 0.437019, 0.428506, 0.419993, 0.411479, 0.405804, 0.402966, 0.391615, 0.383101, 0.37175, 0.360399, 0.360399, 0.351886, 0.334859, 0.329183, 0.326346, 0.317832, 0.312157, 0.309319, 0.309319, 0.300806, 0.297968, 0.292292, 0.283779, 0.275265, 0.272428, 0.258239, 0.255401, 0.252563, 0.249725, 0.24405, 0.241212, 0.235536, 0.227023, 0.227023, 0.224185, 0.21851, 0.21851, 0.209996, 0.207159, 0.198645, 0.198645, 0.19297, 0.184456, 0.181618, 0.181618, 0.173105, 0.175943, 0.170267, 0.16743, 0.161754, 0.161754, 0.161754, 0.161754, 0.156078, 0.150403, 0.147565, 0.144727, 0.144727, 0.136214, 0.133376, 0.1277, 0.124863, 0.122025, 0.119187, 0.113512, 0.110674, 0.110674, 0.104998, 0.104998, 0.10216, 0.0993226, 0.0964848, 0.093647, 0.0964848, 0.0964848, 0.093647, 0.0879714, 0.0879714, 0.0822959, 0.0794581, 0.0766203, 0.0737825, 0.0709447, 0.0709447, 0.0652691, 0.0652691, 0.0624313, 0.0624313, 0.0595936, 0.0567558, 0.0567558, 0.0510802, 0.0482424, 0.0482424, 0.0510802, 0.0482424, 0.0454046, 0.0425668, 0.039729, 0.039729, 0.0425668, 0.0340535, 0.0312157, 0.0312157, 0.0312157, 0.0283779, 0.0283779, 0.0255401, 0.0255401, 0.0283779, 0.0255401, 0.0255401, 0.0198645, 0.0198645, 0.0198645, 0.0198645, 0.0227023, 0.0198645, 0.0198645, 0.0198645, 0.0141889, 0.0141889, 0.0141889, 0.0141889, 0.0113512, 0.0113512, 0.0141889, 0.0113512, 0.0141889, 0.00851337, 0.00851337, 0.00567558, 0.00283779, 0.00851337, 0.00851337, 0.00851337, 0.00851337, 0.00851337, 0.00851337, 0.00283779, 0.00283779, 0.00851337, 0.00283779, 0.00567558, 0.00567558, 0.00851337, 0.00567558, 0.00851337, 0.0113512, 0.00851337, 0.0113512, 0.0141889, 0.0170267, 0.0170267, 0.0198645, 0.0227023, 0.0227023, 0.0255401, 0.0227023, 0.0255401, 0.0255401, 0.0312157, 0.0227023, 0.0255401, 0.0312157, 0.0312157, 0.0340535, 0.0340535, 0.039729, 0.0425668, 0.0482424, 0.053918, 0.0482424, 0.053918, 0.053918, 0.0567558,

3

0.0595936, 0.0595936, 0.0624313, 0.0681069, 0.0681069, 0.0709447, 0.0766203, 0.0766203, 0.0908092, 0.0879714, 0.0908092, 0.104998, 0.104998, 0.110674, 0.116349, 0.116349, 0.119187, 0.124863, 0.122025, 0.136214, 0.136214, 0.144727, 0.147565, 0.150403, 0.150403, 0.156078, 0.161754, 0.164592, 0.170267, 0.173105, 0.178781, 0.187294, 0.19297, 0.201483, 0.204321, 0.209996, 0.212834, 0.224185, 0.232699, 0.238374, 0.246888, 0.252563, 0.266752, 0.278103, 0.283779, 0.29513, 0.303643, 0.306481, 0.326346, 0.340535, 0.351886, 0.357561, 0.368913, 0.400128, 0.414317, 0.445533, 0.465397, 0.499451, 0.544855, 0.559044, 0.627151}

8-2169 front shape data in mm (249 points):
r = {-5.10135, -5.09932, -5.09729, -5.09525, -5.09322, -5.09118, -5.08915, -5.08508, -5.08305, -5.08102, -5.07898, -5.07695, -5.07492, -5.07288, -5.07085, -5.06882, -5.06678, -5.06475, -5.05865, -5.05661, -5.05458, -5.05255, -5.05051, -5.04848, -5.04645, -5.04645, -5.01594, -4.98544, -4.95493, -4.92443, -4.89189, -4.84918, -4.81665, -4.75767, -4.70073, -4.66819, -4.62955, -4.59295, -4.56244, -4.52177, -4.47703, -4.44449, -4.39568, -4.32451, -4.28384, -4.23096, -4.18622, -4.13538, -4.08657, -4.04793, -4.0093, -3.96456, -3.93405, -3.90151, -3.84254, -3.7795, -3.74696, -3.70222, -3.65138, -3.61274, -3.5619, -3.51919, -3.48055, -3.44801, -3.38294, -3.32803, -3.26499, -3.21618, -3.17551, -3.14297, -3.08603, -3.04942, -2.99655, -2.95791, -2.9152, -2.87453, -2.81352, -2.75658, -2.69354, -2.63863, -2.60813, -2.54915, -2.48611, -2.45154, -2.39866, -2.35799, -2.29495, -2.25428, -2.17496, -2.13633, -2.07938, -2.04481, -1.98177, -1.93906, -1.90653, -1.85772, -1.78654, -1.754, -1.70113, -1.65029, -1.60555, -1.55267, -1.4754, -1.41032, -1.36558, -1.31474, -1.26593, -1.21102, -1.15612, -1.10731, -1.05444, -1.0097, -0.964956, -0.908014, -0.844972, -0.771761, -0.710753, -0.661946, -0.609071, -0.546029, -0.482986, -0.436213, -0.393507, -0.352834, -0.301994, 0.346733, 0.385372, 0.446381, 0.503323, 0.543995, 0.5806, 0.613139, 0.668046, 0.700584, 0.78193, 0.836837, 0.87751, 0.936485, 0.99546, 1.03613, 1.07274, 1.16018, 1.22119, 1.28424, 1.31881, 1.37575, 1.42456, 1.47336, 1.5242, 1.56894, 1.60555, 1.65029, 1.7174, 1.7662, 1.80484, 1.85365, 1.89026, 1.93906, 1.9838, 2.03464, 2.08752, 2.11802, 2.17903, 2.20954, 2.28681, 2.33765, 2.41086, 2.46577, 2.51051, 2.55525, 2.62033, 2.6732, 2.73218, 2.78709, 2.83386, 2.87046, 2.9152, 2.95791, 3.01078, 3.06366, 3.12263, 3.16534, 3.23245, 3.27312, 3.32193, 3.35243, 3.39311, 3.43988, 3.48055, 3.53749, 3.57613, 3.64121, 3.69205, 3.75306, 3.7917, 3.87304, 3.92998, 3.96049, 4.02353, 4.06827, 4.11708, 4.15572, 4.21673, 4.27163, 4.3062, 4.35705, 4.42619, 4.46483, 4.49533, 4.536, 4.57871, 4.61125, 4.66209, 4.69463, 4.72717, 4.76174, 4.80648, 4.86749, 4.90409, 4.93866, 4.9712, 5.00171, 5.03221, 5.05661, 5.05865, 5.06068, 5.06271, 5.06475, 5.06678, 5.06882, 5.07085, 5.07288, 5.07492, 5.07695, 5.07898, 5.08102, 5.08305, 5.08508, 5.08712, 5.08915, 5.09118, 5.09322, 5.09525, 5.09729, 5.09932, 5.10135, 5.10339, 5.10542}
z= {0.428142, 0.428142, 0.428142, 0.428142, 0.428142, 0.422471, 0.413965, 0.413965, 0.413965, 0.411129, 0.422471, 0.411129, 0.4168, 0.4168, 0.422471, 0.411129, 0.411129, 0.413965, 0.411129, 0.405459, 0.405459, 0.405459, 0.405459, 0.405459, 0.405459, 0.405459, 0.399788, 0.382776, 0.377105, 0.365763, 0.354422, 0.345916, 0.34308, 0.34308, 0.328903, 0.320397, 0.311891, 0.30622, 0.303385, 0.292044, 0.294879, 0.280702, 0.277867, 0.275031, 0.26369, 0.260854, 0.255184, 0.243842, 0.246678, 0.235336, 0.235336, 0.223995, 0.221159, 0.218324, 0.212653, 0.209818, 0.215488, 0.201312, 0.198476, 0.192805, 0.184299, 0.175793, 0.164452, 0.161616, 0.161616, 0.164452, 0.158781, 0.158781, 0.155946, 0.158781, 0.144604, 0.147439, 0.141769, 0.133263, 0.127592, 0.121921, 0.121921, 0.11625, 0.11625, 0.11625, 0.107744, 0.107744, 0.0992381, 0.0992381, 0.0964027, 0.0935673, 0.0964027, 0.0850612, 0.090732, 0.090732, 0.090732, 0.0850612, 0.0822259, 0.0793905, 0.0793905, 0.0765551, 0.0708844, 0.0708844, 0.0652136, 0.068049, 0.0708844, 0.0538721, 0.0567075, 0.0595429, 0.0482014, 0.0482014, 0.0510367, 0.045366, 0.0482014, 0.045366, 0.0425306, 0.0396952, 0.0425306, 0.0368599, 0.0368599, 0.0340245, 0.0396952, 0.0283537, 0.0311891, 0.0283537, 0.022683, 0.0255184, 0.022683, 0.0283537, 0.0255184, 0.0141769, 0.0141769, 0.0141769, 0.0113415, 0.0141769, 0.0141769, 0.00567075, 0.00850612, 0.00850612, 0.00283537, 0.00567075, 0.00567075, 0.00850612, 0.00850612, 0.0113415, 0.0113415, 0.00850612, 0.0113415, 0.00850612, 0.0113415, 0.00850612, 0.0113415, 0.00567075, 0.00850612, 0.00850612, 0.00850612, 0.00283537, 0.00850612, 0.00850612, 0.00567075, 0.00850612, 0.0113415, 0.00850612, 0.0113415, 0.00850612, 0.0113415, 0.0141769, 0.0141769, 0.0113415, 0.0170122, 0.0170122, 0.0170122, 0.022683, 0.0198476, 0.0198476, 0.0255184, 0.0255184, 0.0340245, 0.0311891, 0.0340245, 0.0340245, 0.0311891, 0.0340245, 0.0396952, 0.045366, 0.0425306, 0.045366, 0.045366, 0.0567075, 0.0567075, 0.0567075, 0.0595429, 0.0652136, 0.0652136, 0.0737197, 0.0793905, 0.0793905, 0.0822259, 0.0850612, 0.0935673, 0.0964027, 0.0964027, 0.102073, 0.104909, 0.113415, 0.119086, 0.124756, 0.130427, 0.133263, 0.144604, 0.155946, 0.158781, 0.167287, 0.175793, 0.181464, 0.187135, 0.18997, 0.201312, 0.201312, 0.218324, 0.229665, 0.232501, 0.243842, 0.260854, 0.277867, 0.297714, 0.30055, 0.30622, 0.303385, 0.323233, 0.323233, 0.326068, 0.323233, 0.328903, 0.328903, 0.328903, 0.331739, 0.334574, 0.33741, 0.348751, 0.348751, 0.348751, 0.345916, 0.34308, 0.340245, 0.340245, 0.348751, 0.357257, 0.357257, 0.357257}

8-2170 front shape data in mm (251 points):
r = {-2.83814, -2.837, -2.83245, -2.83132, -2.82335, -2.82222, -2.82108, -2.81994, -2.81881, -2.81426, -2.81312, -2.81198, -2.81084, -2.80971, -2.80857, -2.80743, -2.8063, -2.80516, -2.80402, -2.80288, -2.80175, -2.80061, -2.79947, -2.79833, -2.7972, -2.7972, -2.75967, -2.74716, -2.71304, -2.70053, -2.65503, -2.63911, -2.61523, -2.60272, -2.57315, -2.53675, -2.52424, -2.50718, -2.48785, -2.43099, -2.4071, -2.3582, -2.33886, -2.32067, -2.28768, -2.25584, -2.23878, -2.21831, -2.20011, -2.14097, -2.11481, -2.08411, -2.06364, -2.05113, -2.02611, -1.98289, -1.96355, -1.93171, -1.9192, -1.901, -1.86347, -1.8248, -1.77817, -1.75088, -1.71562, -1.70311, -1.68605, -1.65534, -1.63601, -1.59962, -1.56436, -1.53593, -1.51773, -1.50181, -1.4802, -1.44153, -1.41082, -1.3949, -1.34941, -1.32894, -1.31074, -1.28458, -1.26411, -1.24023, -1.21066, -1.18564, -1.1663, -1.12081, -1.09693, -1.0685, -1.02414, -0.98661, -0.966139, -0.916098, -0.88539, -0.861507, -0.827388, -0.786445, -0.763699, -0.747777, -0.710246, -0.693186, -0.668165, -0.631772, -0.589692, -0.571495, -0.540788, -0.512355, -0.496433, -0.468, -0.431606, -0.41341, -0.397487, -0.375879, -0.345171, -0.326975, -0.30764, -0.270109, -0.254187, -0.222343, -0.207558, -0.185949, -0.162066, -0.140457, -0.112024, -0.0562965, -0.0267266, 0.0153536, 0.039237, 0.0926902, 0.119985, 0.157516, 0.173439, 0.20642, 0.230304, 0.266698, 0.303091, 0.322425, 0.36678, 0.395213, 0.423645, 0.449803, 0.481648, 0.51008, 0.552161, 0.573769, 0.614712, 0.671577, 0.689774, 0.704559, 0.720481, 0.747777, 0.781896, 0.797818, 0.828525, 0.853546, 0.884253, 0.901313, 0.936569, 0.98661, 1.01277, 1.03779, 1.07987, 1.09465, 1.12991, 1.16403, 1.2027, 1.24364, 1.26411, 1.29709, 1.33008, 1.34259, 1.38467, 1.41082, 1.43584, 1.45859, 1.4893, 1.51546, 1.56891, 1.58597, 1.6235, 1.65989, 1.70311, 1.72245, 1.73723, 1.76225, 1.78727, 1.83276, 1.87029, 1.90555, 1.92034, 1.95332, 1.98061, 1.9954, 2.02724, 2.04544, 2.08638, 2.10913, 2.13415, 2.15462, 2.16713, 2.1967, 2.22968, 2.27404, 2.29223, 2.32863, 2.35365, 2.37639, 2.40255, 2.4344, 2.45259, 2.46965, 2.49012, 2.50264, 2.51856, 2.54813, 2.56632, 2.59021, 2.61523, 2.6448, 2.65731, 2.66982, 2.70621, 2.72213, 2.7517, 2.78582, 2.78924, 2.79037, 2.79151, 2.79606, 2.7972, 2.79833, 2.79947, 2.80061, 2.80288, 2.80402, 2.80516, 2.8063, 2.80743, 2.81426, 2.81539, 2.81653, 2.81767, 2.81881, 2.82335, 2.82449, 2.83245, 2.83359, 2.83814, 2.83928, 2.84041}
z= {0.290667, 0.285023, 0.282201, 0.279379, 0.279379, 0.282201, 0.282201, 0.290667, 0.290667, 0.287845, 0.285023, 0.282201, 0.282201, 0.282201, 0.285023, 0.285023, 0.285023, 0.285023, 0.276557, 0.282201, 0.282201, 0.285023, 0.282201, 0.276557, 0.270913, 0.270913, 0.262447, 0.262447, 0.245515, 0.245515, 0.231405, 0.231405, 0.225761, 0.220117, 0.214473, 0.211651, 0.206007, 0.200363, 0.186253, 0.174965, 0.177787, 0.163677, 0.160855, 0.166499, 0.158033, 0.158033, 0.146745, 0.146745, 0.141101, 0.138279, 0.138279, 0.129813, 0.129813, 0.124169, 0.124169, 0.118525, 0.121347, 0.107236, 0.104414, 0.104414, 0.0987704, 0.0959484, 0.0987704, 0.0959484, 0.0959484, 0.0903044, 0.0818384, 0.0874824, 0.0818384, 0.0761943, 0.0790164, 0.0705503, 0.0705503, 0.0761943, 0.0649063, 0.0620843, 0.0649063, 0.0620843, 0.0564403, 0.0536182, 0.0564403, 0.0536182, 0.0479742, 0.0507962, 0.0564403, 0.0479742, 0.0451522, 0.0479742, 0.0507962, 0.0479742, 0.0479742, 0.0395082, 0.0395082, 0.0366862, 0.0395082, 0.0310421, 0.0366862, 0.0310421, 0.0253981, 0.0225761, 0.0310421, 0.0338642, 0.0197541, 0.0225761, 0.0225761, 0.0253981, 0.0197541, 0.0225761, 0.0225761, 0.0225761, 0.0197541, 0.0197541, 0.0141101, 0.0169321, 0.0141101, 0.0112881, 0.0112881, 0.0112881, 0.0141101, 0.0169321, 0.0169321, 0.00846604, 0.00846604, 0.00846604, 0.0112881, 0.0112881, 0.00846604, 0.00564403, 0.00846604, 0.00846604, 0.0112881, 0.00564403, 0.0112881, 0.00846604, 0.00846604, 0.00282201, 0.0112881, 0.0112881, 0.00846604, 0.00282201, 0.0112881, 0.0169321, 0.0112881, 0.00846604, 0.0141101, 0.00846604, 0.00846604, 0.0141101, 0.0112881, 0.00564403, 0.00282201, 0.0197541, 0.0197541, 0.0141101, 0.0169321, 0.0112881, 0.0282201, 0.0225761, 0.0141101, 0.0282201, 0.0225761, 0.0225761, 0.0225761, 0.0282201, 0.0282201, 0.0253981, 0.0253981, 0.0338642, 0.0338642, 0.0338642, 0.0395082, 0.0366862, 0.0366862, 0.0423302, 0.0451522, 0.0423302, 0.0423302, 0.0451522, 0.0451522, 0.0479742, 0.0507962, 0.0507962, 0.0592623, 0.0536182, 0.0592623, 0.0536182, 0.0620843, 0.0620843, 0.0620843, 0.0592623, 0.0677283, 0.0677283, 0.0705503, 0.0761943, 0.0790164, 0.0761943, 0.00846604, 0.0931264, 0.0959484, 0.0987704, 0.0931264, 0.0987704, 0.101592, 0.110058, 0.118525, 0.110058, 0.121347, 0.129813, 0.126991, 0.135457, 0.135457, 0.141101, 0.143923, 0.135457, 0.155211, 0.155211, 0.160855, 0.163677, 0.172143, 0.174965, 0.194719, 0.206007, 0.200363, 0.200363, 0.197541, 0.206007, 0.206007, 0.208829, 0.208829, 0.208829, 0.211651, 0.211651, 0.208829, 0.208829, 0.211651, 0.217295, 0.217295, 0.211651, 0.220117, 0.220117, 0.217295, 0.214473, 0.214473, 0.222939,

4

0.222939, 0.220117, 0.225761}

8-2171 front shape data in mm (256 points):
r = {-1.93269, -1.92003, -1.91877, -1.91624, -1.91497, -1.91371, -1.91244, -1.91118, -1.90991, -1.90865, -1.90738, -1.90611, -1.90485, -1.90232, -1.90105, -1.89852, -1.89726, -1.89599, -1.89473, -1.89346, -1.8922, -1.88587, -1.88334, -1.87954, -1.87701, -1.87701, -1.86057, -1.85044, -1.83779, -1.82767, -1.81249, -1.79098, -1.78212, -1.76947, -1.75428, -1.73783, -1.72645, -1.71759, -1.70494, -1.68976, -1.67331, -1.66065, -1.62143, -1.61004, -1.58727, -1.57588, -1.56196, -1.55184, -1.51388, -1.49617, -1.48225, -1.47213, -1.44809, -1.43417, -1.41266, -1.40254, -1.38989, -1.36332, -1.34813, -1.33042, -1.3203, -1.29246, -1.27981, -1.26969, -1.26083, -1.24438, -1.2292, -1.20136, -1.17479, -1.16088, -1.13304, -1.12039, -1.109, -1.09508, -1.08116, -1.06345, -1.04953, -1.03941, -1.02802, -1.01537, -0.993862, -0.977414, -0.949578, -0.93566, -0.917946, -0.883784, -0.86101, -0.845826, -0.824317, -0.809134, -0.793951, -0.761054, -0.733218, -0.724362, -0.700322, -0.688934, -0.671221, -0.653507, -0.64465, -0.635793, -0.611753, -0.595305, -0.581387, -0.561143, -0.538368, -0.518124, -0.502941, -0.480166, -0.461187, -0.4498, -0.439678, -0.427025, -0.391598, -0.380211, -0.371354, -0.35364, -0.330866, -0.319478, -0.295438, -0.270133, -0.258746, -0.237236, -0.223318, -0.195483, -0.167647, -0.147403, -0.13475, -0.117037, -0.104384, -0.0879356, -0.0600999, -0.0385904, -0.0272031, -0.00063263, 0.00822419, 0.0360599, 0.100588, 0.115771, 0.127159, 0.138546, 0.170178, 0.196748, 0.213196, 0.223318, 0.258746, 0.287847, 0.300499, 0.323274, 0.340988, 0.35364, 0.370089, 0.378945, 0.410577, 0.448535, 0.47637, 0.485227, 0.511798, 0.526981, 0.54849, 0.573796, 0.599101, 0.62061, 0.630732, 0.661098, 0.669955, 0.680077, 0.707913, 0.729423, 0.749667, 0.761054, 0.774972, 0.793951, 0.806603, 0.843296, 0.867336, 0.879989, 0.890111, 0.902763, 0.940721, 0.963496, 0.973618, 0.982475, 1.01031, 1.01917, 1.03055, 1.05586, 1.0761, 1.10014, 1.11406, 1.13178, 1.14063, 1.15202, 1.171, 1.18492, 1.20516, 1.24565, 1.27222, 1.28234, 1.29626, 1.30765, 1.33928, 1.36205, 1.3823, 1.40128, 1.41266, 1.42911, 1.44809, 1.45948, 1.4734, 1.48352, 1.50882, 1.52907, 1.53792, 1.56323, 1.57209, 1.5936, 1.61257, 1.62776, 1.648, 1.65686, 1.66572, 1.68849, 1.7138, 1.72392, 1.7391, 1.7682, 1.77832, 1.81375, 1.8302, 1.83906, 1.85803, 1.86563, 1.86689, 1.86816, 1.89726, 1.89852, 1.89979, 1.90105, 1.90232, 1.90358, 1.90485, 1.90611, 1.90991, 1.91118, 1.9175, 1.92256, 1.92383, 1.92509, 1.92636, 1.92762, 1.92889, 1.93015, 1.93142, 1.93269, 1.93395, 1.93522}
z= {0.276557, 0.262447, 0.262447, 0.265269, 0.265269, 0.259625, 0.259625, 0.259625, 0.253981, 0.253981, 0.253981, 0.253981, 0.251159, 0.248337, 0.248337, 0.248337, 0.248337, 0.251159, 0.251159, 0.251159, 0.251159, 0.251159, 0.251159, 0.251159, 0.251159, 0.251159, 0.237049, 0.234227, 0.231405, 0.225761, 0.220117, 0.211651, 0.208829, 0.214473, 0.203185, 0.203185, 0.203185, 0.197541, 0.186253, 0.183431, 0.189075, 0.183431, 0.158033, 0.163677, 0.163677, 0.163677, 0.166499, 0.160855, 0.138279, 0.143923, 0.138279, 0.146745, 0.135457, 0.135457, 0.138279, 0.135457, 0.126991, 0.121347, 0.124169, 0.121347, 0.121347, 0.110058, 0.115703, 0.101592, 0.104414, 0.104414, 0.0959484, 0.101592, 0.0959484, 0.0903044, 0.0874824, 0.0931264, 0.0959484, 0.0959484, 0.0846604, 0.0818384, 0.0818384, 0.0818384, 0.0677283, 0.0705503, 0.0705503, 0.0705503, 0.0677283, 0.0790164, 0.0761943, 0.0677283, 0.0649063, 0.0649063, 0.0507962, 0.0592623, 0.0564403, 0.0649063, 0.0592623, 0.0564403, 0.0536182, 0.0479742, 0.0592623, 0.0507962, 0.0451522, 0.0479742, 0.0507962, 0.0479742, 0.0395082, 0.0451522, 0.0366862, 0.0395082, 0.0423302, 0.0395082, 0.0366862, 0.0395082, 0.0366862, 0.0310421, 0.0282201, 0.0282201, 0.0451522, 0.0310421, 0.0338642, 0.0366862, 0.0253981, 0.0282201, 0.0225761, 0.0282201, 0.0197541, 0.0310421, 0.0282201, 0.0253981, 0.0225761, 0.0141101, 0.0225761, 0.0225761, 0.0310421, 0.0141101, 0.0282201, 0.0253981, 0.0197541, 0.0112881, 0.0169321, 0.0253981, 0.0253981, 0.0253981, 0.0112881, 0.0169321, 0.0253981, 0.0225761, 0.0253981, 0.00846604, 0.0282201, 0.0197541, 0.0225761, 0.0169321, 0.0169321, 0.0112881, 0.0141101, 0.0141101, 0.00564403, 0., 0.00846604, 0.0112881, 0.0169321, 0.0225761, 0.0253981, 0.0225761, 0.0225761, 0.0338642, 0.0310421, 0.0253981, 0.0225761, 0.0253981, 0.0282201, 0.0310421, 0.0338642, 0.0338642, 0.0395082, 0.0366862, 0.0423302, 0.0366862, 0.0338642, 0.0395082, 0.0451522, 0.0451522, 0.0507962, 0.0451522, 0.0479742, 0.0507962, 0.0507962, 0.0536182, 0.0536182, 0.0479742, 0.0536182, 0.0564403, 0.0479742, 0.0479742, 0.0507962, 0.0507962, 0.0677283, 0.0677283, 0.0705503, 0.0649063, 0.0705503, 0.0733723, 0.0761943, 0.0818384, 0.0705503, 0.0705503, 0.0846604, 0.0903044, 0.0874824, 0.0903044, 0.0931264, 0.0818384, 0.0987704, 0.0987704, 0.101592, 0.0959484, 0.118525, 0.115703, 0.112881, 0.118525, 0.121347, 0.121347, 0.129813, 0.135457, 0.135457, 0.143923, 0.143923, 0.152389, 0.158033, 0.158033, 0.158033, 0.158033, 0.169321, 0.172143, 0.169321, 0.166499, 0.166499, 0.169321, 0.169321, 0.174965, 0.172143, 0.169321, 0.174965, 0.180609, 0.180609, 0.177787, 0.180609, 0.186253, 0.186253, 0.180609, 0.180609, 0.180609, 0.180609, 0.180609}

8-2172 front shape data in mm (247 points):
r = {-12.4974, -12.4951, -12.4927, -12.4904, -12.4881, -12.4857, -12.4834, -12.4811, -12.4764, -12.4741, -12.4718, -12.4694, -12.4671, -12.4648, -12.4624, -12.4601, -12.4578, -12.4554, -12.4531, -12.4508, -12.4485, -12.4461, -12.4438, -12.4415, -12.4391, -12.4391, -12.3483, -12.2667, -12.1409, -12.057, -11.9009, -11.8123, -11.6958, -11.6026, -11.5141, -11.4186, -11.33, -11.2275, -11.1226, -11.0178, -10.9176, -10.7988, -10.7149, -10.5984, -10.4912, -10.3793, -10.2302, -10.137, -10.0368, -9.9343, -9.80848, -9.68498, -9.55916, -9.41702, -9.29819, -9.12343, -9.01159, -8.88576, -8.76227, -8.62712, -8.51528, -8.38713, -8.21237, -8.09121, -7.97936, -7.86053, -7.73237, -7.62985, -7.48538, -7.40383, -7.24306, -7.11956, -6.98675, -6.8283, -6.69316, -6.58597, -6.47646, -6.33899, -6.24112, -6.13627, -5.98481, -5.86831, -5.74015, -5.61899, -5.50482, -5.38831, -5.31142, -5.1786, -5.0155, -4.85938, -4.73822, -4.6054, -4.50288, -4.34211, -4.21628, -4.12075, -3.94133, -3.83182, -3.72696, -3.59648, -3.47532, -3.37046, -3.24231, -3.11881, -2.99066, -2.87182, -2.72736, -2.62251, -2.48969, -2.37785, -2.25435, -2.09591, -1.99571, -1.85591, -1.76038, -1.59028, -1.48077, -1.38523, -1.28737, -1.16854, -1.05902, -0.951838, -0.800383, -0.688539, -0.567375, -0.413589, -0.278445, 0.742131, 0.886596, 1.05902, 1.15922, 1.29436, 1.39921, 1.51805, 1.66484, 1.78601, 1.9095, 2.02601, 2.1728, 2.29163, 2.42911, 2.56425, 2.6994, 2.81823, 2.91144, 3.04425, 3.15376, 3.26095, 3.37046, 3.54755, 3.66172, 3.79454, 3.90871, 4.05551, 4.17667, 4.34444, 4.47958, 4.59608, 4.74055, 4.85938, 4.96424, 5.09938, 5.19725, 5.33239, 5.4652, 5.61433, 5.76812, 5.90093, 6.03141, 6.17122, 6.28539, 6.45316, 6.55102, 6.68384, 6.80966, 6.92151, 7.04966, 7.15917, 7.28966, 7.45509, 7.56228, 7.69043, 7.83257, 7.94907, 8.06558, 8.18208, 8.33819, 8.45237, 8.55023, 8.70402, 8.85314, 8.97897, 9.10945, 9.23295, 9.37042, 9.46595, 9.57081, 9.67333, 9.7945, 9.92032, 10.0112, 10.116, 10.1976, 10.3281, 10.4446, 10.5378, 10.6869, 10.8221, 10.9549, 11.1017, 11.1972, 11.3323, 11.4442, 11.5327, 11.6632, 11.7681, 11.8543, 11.9405, 12.036, 12.1269, 12.2224, 12.3133, 12.4088, 12.4112, 12.4135, 12.4158, 12.4182, 12.4205, 12.4228, 12.4252, 12.4275, 12.4298, 12.4321, 12.4368, 12.4624, 12.4648, 12.4671, 12.4694, 12.4718, 12.4741, 12.4764, 12.4787, 12.4811, 12.4951, 12.4974, 12.4997, 12.502}
z= {0.547821, 0.539306, 0.536467, 0.533629, 0.533629, 0.527952, 0.533629, 0.533629, 0.525113, 0.525113, 0.525113, 0.525113, 0.519436, 0.519436, 0.516598, 0.516598, 0.513759, 0.513759, 0.508083, 0.513759, 0.516598, 0.513759, 0.513759, 0.513759, 0.510921, 0.510921, 0.47686, 0.471183, 0.437121, 0.422929, 0.400221, 0.397383, 0.380352, 0.377514, 0.363322, 0.351968, 0.349129, 0.333497, 0.332099, 0.320745, 0.31223, 0.306553, 0.300876, 0.300876, 0.286683, 0.283845, 0.27533, 0.269653, 0.266814, 0.258299, 0.249784, 0.244107, 0.244107, 0.23843, 0.232753, 0.227076, 0.215722, 0.218561, 0.207207, 0.207207, 0.20153, 0.193015, 0.193015, 0.198692, 0.184499, 0.184499, 0.173145, 0.181661, 0.173145, 0.161792, 0.156115, 0.153276, 0.156115, 0.153276, 0.150438, 0.147599, 0.144761, 0.147599, 0.133407, 0.130569, 0.133407, 0.12773, 0.119215, 0.113538, 0.122053, 0.1107, 0.107861, 0.0993458, 0.0993458, 0.0993458, 0.0936689, 0.0908304, 0.0908304, 0.0851535, 0.082315, 0.0766381, 0.0794766, 0.0709612, 0.0709612, 0.0709612, 0.0709612, 0.0709612, 0.056769, 0.056769, 0.056769, 0.056769, 0.0482536, 0.0482536, 0.0510921, 0.0510921, 0.0397383, 0.0397383, 0.0368999, 0.0454152, 0.0425768, 0.0425768, 0.0368999, 0.0312229, 0.0340614, 0.0312229, 0.0340614, 0.0312229, 0.0340614, 0.0283845, 0.025546, 0.0340614, 0.0141922, 0.0170307, 0.0198692, 0.0198692, 0.0227076, 0.0198692, 0.0141922, 0.0113538, 0.00851535, 0.00851535, 0.0113538, 0.0056769, 0.0056769, 0.00851535, 0.00851535, 0.0056769, 0., 0.00283845, 0.00851535, 0.00851535, 0.00283845, 0.0056769, 0.0113538, 0.0056769, 0.00851535, 0.0113538, 0.0113538, 0.0141922, 0.0113538, 0.0113538, 0.0113538, 0.0141922, 0.0141922, 0.0170307, 0.0198692, 0.0198692, 0.0198692, 0.0227076, 0.0227076, 0.025546, 0.0283845, 0.0283845, 0.0340614, 0.0340614, 0.0340614, 0.0397383, 0.0368999, 0.0397383, 0.0482536, 0.0482536, 0.0539305, 0.0624459, 0.0596074, 0.0652843, 0.0681228, 0.0737997, 0.0766381, 0.0794766, 0.0794766, 0.0851535, 0.0851535, 0.102184, 0.105023, 0.105023, 0.1107, 0.119215, 0.116376, 0.122053, 0.12773, 0.136246, 0.139084, 0.141922, 0.147599, 0.153276, 0.161792, 0.16463, 0.161792, 0.178822, 0.187338, 0.190176, 0.195853, 0.207207, 0.215722, 0.215722, 0.221399, 0.232753, 0.23843, 0.246945, 0.252622, 0.261137, 0.281007, 0.283845, 0.286683, 0.283845, 0.283845, 0.289522, 0.289522, 0.286683, 0.283845, 0.283845, 0.283845, 0.289522, 0.295199, 0.286683, 0.286683, 0.289522, 0.286683, 0.286683, 0.286683, 0.289522, 0.286683, 0.286683, 0.289522, 0.298037, 0.298037, 0.300876}

1.3. Cylinder Expansion Wall Motion Records

8-2172 PDV records with t in μs and v_r (wall velocity component normal to probe) in mm/μs:
(Probe azimuthal locations θ are reported relative to PDV 1)
Averaged PDV trace (243 points):
$t = \{$0., 0.01664, 0.0512, 0.0832, 0.10752, 0.13952, 0.1792, 0.22144, 0.2432, 0.28672, 0.32128, 0.37248, 0.40192, 0.44928, 0.4992, 0.53632, 0.59904, 0.6592, 0.736, 0.76544, 0.77696, 0.8128, 0.86912, 0.89088, 0.91648, 0.9472, 0.95872, 0.96768, 0.9728, 0.97536, 0.97792, 0.98048, 0.98304, 0.9856, 0.98816, 0.99072, 0.99584, 0.99968, 1.00224, 1.00992, 1.01376, 1.0176, 1.024, 1.03168, 1.0368, 1.0624, 1.07392, 1.09056, 1.10848, 1.13792, 1.15328, 1.19808, 1.24544, 1.25696, 1.27872, 1.29664, 1.32736, 1.36448, 1.38368, 1.40288, 1.43488, 1.47456, 1.4912, 1.52448, 1.55904, 1.6, 1.63456, 1.69984, 1.73824, 1.77152, 1.80736, 1.84064, 1.85984, 1.88416, 1.90592, 1.91616, 1.9392, 1.94944, 1.95712, 1.96352, 1.96992, 1.9776, 1.98272, 1.98784, 1.99168, 1.99424, 1.99936, 2.02112, 2.0352, 2.05312, 2.06848, 2.12352, 2.18368, 2.21312, 2.26048, 2.3232, 2.36672, 2.41152, 2.43584, 2.46784, 2.50752, 2.54848, 2.6048, 2.63936, 2.7008, 2.7264, 2.76096, 2.79296, 2.80064, 2.81856, 2.83392, 2.85056, 2.87104, 2.90304, 2.92224, 2.95552, 2.97216, 2.99904, 3.06176, 3.1168, 3.21408, 3.26656, 3.32928, 3.36128, 3.41504, 3.4816, 3.5392, 3.59552, 3.63904, 3.65696, 3.70048, 3.7184, 3.76192, 3.80416, 3.83744, 3.88096, 3.95648, 4.03072, 4.08064, 4.14464, 4.18048, 4.23424, 4.29568, 4.3584, 4.44416, 4.48768, 4.52864, 4.55808, 4.59904, 4.65536, 4.73984, 4.86272, 4.91648, 4.992, 5.08288, 5.18912, 5.24032, 5.30688, 5.37984, 5.42848, 5.54496, 5.64224, 5.71136, 5.83808, 5.94688, 6.01088, 6.07104, 6.17472, 6.33216, 6.4448, 6.61632, 6.72256, 6.84416, 7.01056, 7.15776, 7.34848, 7.43936, 7.63904, 7.83744, 8.02816, 8.24064, 8.45312, 8.64768, 8.78336, 9.0432, 9.216, 9.51296, 9.71008, 9.952, 10.1683, 10.4166, 10.6125, 10.7354, 11.0093, 11.223, 11.3971, 11.584, 11.7325, 11.7965, 11.8797, 12.1024, 12.3174, 12.5146, 12.7821, 13.0317, 13.3005, 13.5757, 13.8675, 14.0992, 14.2963, 14.5574, 14.7507, 15.0144, 15.3229, 15.5277, 15.7094, 15.9654, 16.2611, 16.5325, 16.8102, 17.0714, 17.1622, 17.2621, 17.3645, 17.5782, 17.792, 17.9712, 18.0685, 18.2323, 18.5331, 18.775, 19.0323, 19.1949, 19.2998, 19.5584, 19.6442, 19.9078, 20.1754, 20.3802, 20.5709, 20.7987, 20.8154, 20.8166$\}$
$v_r = \{$0.894766, 0.895536, 0.887686, 0.886266, 0.87813, 0.871853, 0.860958, 0.87052, 0.854516, 0.842897, 0.836395, 0.824782, 0.813338, 0.810821, 0.797936, 0.790928, 0.784248, 0.773077, 0.775156, 0.781404, 0.793381, 0.797474, 0.787734, 0.798067, 0.808264, 0.820238, 0.831289, 0.842065, 0.853494, 0.859357, 0.867634, 0.880814, 0.892627, 0.907996, 0.919899, 0.931399, 0.93904, 0.974026, 0.998368, 1.01738, 1.08243, 1.11581, 1.13458, 1.14784, 1.15898, 1.16929, 1.18561, 1.19288, 1.18861, 1.19611, 1.18692, 1.18989, 1.19335, 1.19355, 1.1831, 1.1831, 1.18098, 1.17744, 1.16915, 1.16709, 1.16011, 1.1566, 1.14456, 1.14361, 1.13638, 1.12866, 1.1312, 1.13002, 1.13656, 1.14676, 1.14971, 1.15992, 1.16335, 1.16681, 1.17656, 1.1876, 1.20046, 1.21063, 1.22404, 1.23349, 1.24557, 1.25643, 1.26753, 1.28066, 1.29198, 1.30022, 1.31596, 1.32478, 1.33582, 1.34782, 1.36009, 1.3661, 1.36244, 1.35818, 1.35784, 1.3593, 1.35296, 1.34853, 1.34514, 1.3346, 1.32377, 1.31706, 1.31133, 1.31273, 1.31639, 1.31606, 1.3274, 1.33826, 1.34813, 1.35952, 1.37033, 1.38348, 1.39456, 1.40723, 1.41823, 1.42685, 1.43869, 1.45165, 1.46374, 1.46153, 1.45466, 1.45083, 1.44104, 1.43571, 1.42377, 1.41401, 1.41479, 1.42361, 1.43444, 1.44667, 1.45697, 1.46894, 1.48121, 1.49056, 1.50292, 1.5147, 1.52043, 1.52494, 1.51517, 1.51018, 1.4989, 1.49287, 1.48342, 1.48713, 1.49634, 1.50836, 1.51996, 1.53135, 1.54005, 1.55023, 1.56082, 1.55702, 1.5486, 1.54376, 1.53567, 1.54011, 1.55162, 1.5794, 1.57206, 1.57922, 1.5876, 1.59895, 1.60927, 1.60871, 1.59991, 1.60385, 1.61564, 1.62581, 1.62669, 1.62232, 1.62919, 1.64071, 1.64302, 1.64228, 1.64962, 1.65591, 1.65656, 1.66529, 1.66943, 1.66829, 1.67624, 1.67856, 1.68222, 1.6879, 1.69133, 1.69576, 1.6982, 1.70126, 1.70352, 1.70725, 1.71124, 1.71207, 1.71591, 1.71174, 1.71733, 1.71964, 1.72275, 1.72474, 1.72771, 1.73128, 1.7352, 1.73736, 1.73956, 1.74556, 1.74709, 1.74949, 1.75158, 1.75361, 1.75532, 1.75717, 1.76164, 1.76088, 1.76467, 1.76669, 1.76611, 1.76984, 1.76783, 1.76925, 1.77087, 1.77221, 1.7738, 1.77303, 1.77503, 1.77532, 1.77662, 1.77877, 1.77681, 1.77817, 1.78053, 1.78103, 1.78106, 1.78197, 1.78211, 1.78336, 1.7871, 1.78536, 1.7853$\}$

PDV 1 at $z = 203$ mm and $\theta = 0^\circ$ (247 points):
$t = \{$0-0.0727, -0.04966, -0.02534, -0.00486, 0.01562, 0.05402, 0.1257, 0.19098, 0.23706, 0.28698, 0.35738, 0.39322, 0.41882, 0.4713, 0.5737, 0.60314, 0.70042, 0.73882, 0.8297, 0.8809, 0.94106, 0.96538, 0.97562, 0.98074, 0.9833, 0.89856, 1.0089, 1.0281, 1.03834, 1.08314, 1.12666, 1.1689, 1.22138, 1.2585, 1.28666, 1.29562, 1.34298, 1.3737, 1.40314, 1.47738, 1.5337, 1.54266, 1.57978, 1.62714, 1.6681, 1.70778, 1.78714, 1.84602, 1.89082, 1.92026, 1.96122, 1.97914, 1.98554, 1.99066, 1.99834, 2.03418, 2.1161, 2.1929, 2.34394, 2.41562, 2.4809, 2.53338, 2.61146, 2.67802, 2.74714, 2.82906, 2.8841, 2.93146, 2.9801, 3.0441, 3.16954, 3.24378, 3.34362, 3.41914, 3.51002, 3.53562, 3.68666, 3.73018, 3.92858, 4.01904, 4.35866, 4.46874, 4.52506, 4.60442, 4.70042, 4.77594, 4.88474, 4.95258, 4.99994, 5.12154, 5.20602, 5.3033, 5.38906, 5.50426, 5.63866, 5.71674, 5.93562, 6.02778, 6.12378, 6.28762, 6.40666, 6.46682, 6.6281, 6.85466, 7.02234, 7.30394, 7.4537, 7.58938, 7.85306, 8.03354, 8.28698, 8.52122, 8.83098, 8.96666, 9.19194, 9.43898, 9.70394, 9.98938, 10.3183, 10.6012, 11.0223, 11.5766, 11.8403, 12.095, 12.5711, 13.5311, 14.2044, 14.6486, 14.8089, 15.0428, 15.3449, 15.7609, 16.2051, 16.4726, 16.7798, 17.2739, 17.8435, 17.9638, 18.038, 18.5219, 18.678, 19.0454, 19.3551, 19.6342, 19.8492, 20.1935, 20.3817, 20.4508, 20.6287, 21.0358, 21.5401, 22.0585, 22.3849, 22.687, 23.1465, 23.2975, 23.4742, 23.9311, 24.095, 24.2947, 24.7209, 25.0742, 25.3135, 26.0342, 26.5155, 27.1235, 27.5036, 27.8467, 28.1948, 28.7555, 29.3007, 29.7347, 30.3606, 30.6652, 30.8585, 31.0953, 31.3551, 31.4601, 31.7199, 32.2742, 32.6326, 32.8284, 32.9244, 33.1958, 33.4607, 33.5606, 33.631, 33.8691, 34.2633, 34.7305, 35.3667, 35.9158, 36.2409, 36.5711, 36.7785, 36.9731, 37.1843, 37.4479, 37.6463, 37.7692, 37.9215, 38.143, 38.3132, 38.5065, 38.6115, 38.6767, 38.7535, 38.8815, 39.3078, 39.8863, 40.0284, 40.1027, 40.1308, 40.1782, 40.3484, 40.7132, 41.3519, 41.9727, 42.2723, 42.7727, 43.1235, 43.3231, 43.6329, 43.8863, 44.0489, 44.214, 44.598, 44.8579, 44.982, 45.055, 45.0806, 45.1292, 45.1548, 45.2649, 45.3583, 45.4454, 45.5324, 45.6745, 45.9791, 46.4591, 46.463, 46.4643$\}$
$v_r = \{$0.854144, 0.848049, 0.841872, 0.868389, 0.892551, 0.868485, 0.87052, 0.853819, 0.838865, 0.823917, 0.815926, 0.816273, 0.812841, 0.793596, 0.783816, 0.779457, 0.763911, 0.763298, 0.778786, 0.790149, 0.819825, 0.84503, 0.857796, 0.891978, 0.913328, 0.934335, 1.12344, 1.1463, 1.17023, 1.18612, 1.18756, 1.19812, 1.1991, 1.18286, 1.17452, 1.15975, 1.18439, 1.17664, 1.15531, 1.14543, 1.13579, 1.11758, 1.1264, 1.11792, 1.12656, 1.13169, 1.13122, 1.14743, 1.17429, 1.18379, 1.21018, 1.23812, 1.25991, 1.28676, 1.32345, 1.35235, 1.36634, 1.35208, 1.33838, 1.31596, 1.29922, 1.30402, 1.32212, 1.36617, 1.3954, 1.4201, 1.44584, 1.46144, 1.45802, 1.44967, 1.43752, 1.42079, 1.40951, 1.40034, 1.42078, 1.44944, 1.47135, 1.49935, 1.52218, 1.51072, 1.49638, 1.47655, 1.48191, 1.50902, 1.53187, 1.54845, 1.55761, 1.55717, 1.54344, 1.53961, 1.52718, 1.53826, 1.55179, 1.5732, 1.58418, 1.58486, 1.57132, 1.58378, 1.60082, 1.61079, 1.59749, 1.59489, 1.60155, 1.62142, 1.626, 1.63321, 1.63613, 1.64014, 1.64831, 1.65323, 1.65614, 1.66401, 1.66776, 1.66829, 1.67207, 1.68648, 1.68907, 1.69576, 1.69817, 1.70659, 1.71391, 1.7174, 1.72015, 1.72585, 1.73158, 1.73298, 1.7413, 1.74231, 1.74541, 1.74186, 1.74926, 1.75136, 1.7533, 1.7606, 1.75863, 1.76034, 1.76448, 1.77143, 1.77277, 1.76832, 1.77473, 1.77477, 1.78115, 1.77949, 1.77226, 1.77349, 1.78018, 1.78313, 1.7871, 1.7871, 1.78946, 1.78857, 1.79261, 1.79346, 1.79275, 1.79457, 1.79702, 1.79592, 1.79673, 1.79795, 1.79778, 1.79508, 1.79732, 1.79998, 1.80251, 1.8038, 1.80571, 1.8046, 1.80872, 1.81145, 1.81342, 1.81465, 1.81545, 1.81807, 1.81551, 1.81558, 1.81954, 1.82054, 1.81945, 1.82018, 1.82289, 1.81991, 1.82106, 1.82412, 1.82135, 1.816, 1.82481, 1.82363, 1.82566, 1.82612, 1.82613, 1.82583, 1.82505, 1.82547, 1.82447, 1.82571, 1.82495, 1.82676, 1.82449, 1.8244, 1.82471, 1.82474, 1.82641, 1.82533, 1.82672, 1.81646, 1.82001, 1.82429, 1.82494, 1.82627, 1.82181, 1.8269, 1.8319, 1.82409, 1.82515, 1.8271, 1.82693, 1.8274, 1.82741, 1.82858, 1.82629, 1.83051, 1.82813, 1.82677, 1.83013, 1.82849, 1.82897, 1.82685, 1.82673, 1.80616, 1.82131, 1.82828, 1.81194, 1.82891, 1.83017, 1.8252, 1.82649, 1.8334, 1.82877, 1.82975, 1.82934, 1.82923$\}$

PDV 2 at $z = 203$ mm and $\theta = 90^\circ$ (248 points):
$t = \{$0., 0.0128, 0.0512, 0.07808, 0.10624, 0.15232, 0.17792, 0.24704, 0.27648, 0.384, 0.42624, 0.49792, 0.52224, 0.59648, 0.704, 0.7488, 0.77696, 0.80512, 0.86912, 0.94208, 0.97408, 0.97664, 0.99712, 1.00864, 1.0368, 1.07008, 1.08928, 1.14176, 1.15328, 1.22496, 1.27232, 1.32352, 1.3568, 1.36832, 1.39904, 1.4528, 1.48736, 1.49632, 1.56032, 1.6384, 1.69728, 1.7408, 1.77536, 1.8112, 1.84576, 1.88032, 1.90848, 1.93792, 1.96352, 1.99296, 2.0096, 2.0352, 2.0736, 2.18368, 2.22208, 2.30016, 2.36672, 2.42816, 2.46144, 2.51776, 2.57664, 2.62016, 2.66624, 2.75328, 2.79552, 2.86336, 2.91968, 2.97984, 3.06176, 3.10656, 3.21024, 3.32544, 3.35104, 3.39968, 3.47648, 3.58912, 3.6992, 3.80544, 3.89376, 3.97312, 4.02432, 4.09472, 4.19968, 4.2816, 4.33152, 4.38144, 4.50688, 4.5696, 4.6272, 4.75904, 4.87168, 4.92544, 5.13792, 5.2992, 5.41184, 5.60256, 5.664, 5.77664, 5.8752, 5.952, 6.03648, 6.208, 6.37952, 6.53824, 6.79936, 7.02976, 7.17184, 7.4176, 7.6288, 7.79264, 8.04736, 8.4096, 8.59264, 8.70272, 8.80768, 9.19552, 9.51808, 9.68064, 9.9392, 10.2298, 10.4346, 10.5971, 10.6957, 10.816, 11.0669, 11.337, 11.5674, 11.7222, 11.7632, 11.8016, 11.8784, 12.1331, 12.3213, 12.4608, 12.6298, 12.8474, 13.1584, 13.4874, 13.76, 14.1184, 14.4384, 14.7494, 15.0643, 15.3779, 15.6083, 15.7811, 16.0486, 16.288, 16.5414, 16.841, 17.0714, 17.1328, 17.1878, 17.2736, 17.344, 17.4336, 17.7126, 17.8483, 17.975, 18.0749, 18.3424, 18.5446, 18.7354, 19.0016, 19.1398, 19.2486, 19.3293, 19.5008, 19.6122, 19.7261, 19.9053, 20.0806, 20.2624,

20.4608, 20.6541, 20.8218, 21.1136, 21.3427, 21.5974, 21.8342, 22.0698, 22.281, 22.4691, 22.5485, 22.6227, 22.7136, 22.8992, 23.1462, 23.2192, 23.4381, 23.6045, 23.8029, 23.8682, 23.9283, 24.0064, 24.1702, 24.3328, 24.4403, 24.5376, 24.7488, 24.9907, 25.1827, 25.312, 25.4029, 25.5411, 25.6973, 25.7882, 25.8586, 25.9469, 26.0928, 26.2502, 26.3859, 26.4448, 26.5754, 26.7302, 26.8954, 27.1078, 27.2499, 27.3907, 27.5456, 27.6723, 27.7491, 27.8797, 28.183, 28.4198, 28.6528, 28.8896, 29.0278, 29.1648, 29.2723, 29.5142, 29.6973, 29.9366, 30.153, 30.2938, 30.3923, 30.624, 30.7622, 30.9325, 31.0861, 31.1974, 31.3446, 31.4483, 31.5981, 31.7094, 31.8042, 31.8554, 31.8566}
v_r= {0.874172, 0.893267, 0.890078, 0.900007, 0.885067, 0.876585, 0.871503, 0.852566, 0.841366, 0.8184, 0.803061, 0.818669, 0.814254, 0.777495, 0.782479, 0.801619, 0.867985, 0.793513, 0.806285, 0.837582, 0.905311, 0.921713, 1.14649, 1.18447, 1.18501, 1.16007, 1.18136, 1.19939, 1.17971, 1.19781, 1.18964, 1.17159, 1.15606, 1.14343, 1.15494, 1.15342, 1.13325, 1.09951, 1.13661, 1.13014, 1.12673, 1.14196, 1.154, 1.17599, 1.18093, 1.16188, 1.17643, 1.19403, 1.26005, 1.29439, 1.3479, 1.35367, 1.37178, 1.37747, 1.36566, 1.3622, 1.35798, 1.3649, 1.34822, 1.31631, 1.31364, 1.31835, 1.31365, 1.32481, 1.34727, 1.39524, 1.41758, 1.44514, 1.47701, 1.4546, 1.46132, 1.44875, 1.42129, 1.42964, 1.41137, 1.42708, 1.46464, 1.49375, 1.51293, 1.52276, 1.51663, 1.5085, 1.50327, 1.49975, 1.48858, 1.4837, 1.50819, 1.54775, 1.55452, 1.56361, 1.56476, 1.52807, 1.53717, 1.56138, 1.57627, 1.58811, 1.57999, 1.57774, 1.57397, 1.5736, 1.58954, 1.60756, 1.60836, 1.60216, 1.62499, 1.63598, 1.62514, 1.63552, 1.64434, 1.64108, 1.65113, 1.65565, 1.66615, 1.66647, 1.66587, 1.67553, 1.6834, 1.68417, 1.68687, 1.69263, 1.69949, 1.68708, 1.70248, 1.70366, 1.70621, 1.70801, 1.7132, 1.71576, 1.7117, 1.71147, 1.71391, 1.71872, 1.72694, 1.7172, 1.72142, 1.72589, 1.72868, 1.72654, 1.73108, 1.7379, 1.74044, 1.74581, 1.7454, 1.74944, 1.74864, 1.75317, 1.75237, 1.75257, 1.76241, 1.76372, 1.75815, 1.76535, 1.76984, 1.75363, 1.76659, 1.7742, 1.76399, 1.76759, 1.77481, 1.77302, 1.77079, 1.77025, 1.77428, 1.77599, 1.77985, 1.76838, 1.77895, 1.77796, 1.76432, 1.77612, 1.77858, 1.77985, 1.78066, 1.78361, 1.7804, 1.7879, 1.79621, 1.79586, 1.79176, 1.80641, 1.78938, 1.80645, 1.8029, 1.80854, 1.80652, 1.80754, 1.80618, 1.79309, 1.79358, 1.80315, 1.80816, 1.81399, 1.80158, 1.80469, 1.81794, 1.81336, 1.81466, 1.81146, 1.8151, 1.81377, 1.81406, 1.81252, 1.81344, 1.82285, 1.81758, 1.82068, 1.81647, 1.82075, 1.81323, 1.81356, 1.82052, 1.81782, 1.81424, 1.82207, 1.82774, 1.82174, 1.81935, 1.826, 1.82547, 1.82717, 1.82688, 1.82057, 1.82372, 1.8256, 1.82233, 1.80757, 1.82566, 1.82562, 1.82926, 1.82499, 1.82407, 1.80712, 1.82452, 1.8222, 1.8207, 1.83134, 1.82388, 1.82026, 1.81011, 1.82628, 1.81552, 1.8216, 1.80505, 1.80498}

PDV 4 at $z = 203$ mm and $\theta = 270°$ (246 points):
t = {0., 0.02176, 0.09088, 0.12672, 0.20096, 0.24576, 0.30848, 0.38016, 0.4864, 0.55808, 0.66432, 0.74752, 0.83968, 0.9216, 0.95872, 0.97536, 0.98816, 0.99712, 1.00224, 1.00608, 1.01632, 1.04832, 1.08544, 1.09312, 1.11616, 1.16864, 1.22112, 1.24544, 1.26976, 1.2864, 1.29664, 1.3184, 1.344, 1.37216, 1.39392, 1.41952, 1.43104, 1.46944, 1.51936, 1.60896, 1.6512, 1.69344, 1.72928, 1.8112, 1.88032, 1.92768, 1.95072, 1.95968, 1.99424, 2.01728, 2.06976, 2.1312, 2.21184, 2.2976, 2.4064, 2.5088, 2.62272, 2.68416, 2.78272, 2.81856, 2.86592, 2.92608, 2.9696, 3.0912, 3.1744, 3.29728, 3.38432, 3.47776, 3.5136, 3.53408, 3.61216, 3.64288, 3.7248, 3.808, 3.87584, 3.96928, 4., 4.032, 4.16896, 4.21504, 4.33152, 4.42752, 4.51072, 4.59904, 4.7104, 4.85888, 5.01888, 5.09312, 5.19552, 5.29152, 5.37856, 5.4272, 5.49888, 5.54368, 5.6128, 5.74464, 5.87264, 5.99168, 6.1504, 6.2784, 6.44096, 6.60736, 6.79936, 6.90432, 6.98752, 7.04384, 7.21664, 7.35616, 7.51232, 7.6672, 7.8464, 8.09472, 8.16256, 8.42368, 8.6528, 8.8576, 9.14304, 9.24032, 9.4912, 9.71264, 9.8816, 10.1082, 10.3514, 10.5229, 10.7379, 10.9133, 11.0656, 11.2141, 11.3587, 11.4138, 11.7043, 12.1101, 12.3674, 12.6758, 12.9677, 13.1149, 13.3261, 13.609, 13.975, 14.0992, 14.1978, 14.4397, 14.6509, 14.8019, 15.0541, 15.2691, 15.5213, 15.7299, 16.279, 16.8422, 17.2518, 17.5603, 17.9123, 18.1056, 18.391, 18.9888, 19.1526, 19.4598, 19.7389, 20.0986, 20.3123, 20.8141, 20.9485, 21.0278, 21.353, 21.7741, 22.0058, 22.2336, 22.5946, 22.9645, 23.0848, 23.3075, 23.6186, 23.9373, 24.3994, 24.6208, 24.919, 25.3069, 25.6192, 25.8778, 26.2384, 26.7187, 27.0502, 27.177, 27.2192, 27.3395, 27.6531, 28.0358, 28.4582, 28.6784, 28.8371, 28.9869, 29.2378, 29.705, 30.135, 30.4179, 30.6317, 30.8301, 31.0912, 31.4227, 31.7005, 31.8861, 32.1382, 32.3379, 32.4019, 32.585, 32.7091, 32.8678, 33.0291, 33.1866, 33.3043, 33.449, 33.6192, 33.7229, 33.8048, 33.9597, 34.2298, 34.4205, 34.5946, 34.6701, 34.7674, 34.8723, 34.9965, 35.0797, 35.232, 35.4317, 35.6186, 35.785, 35.9654, 36.151, 36.3226, 36.5594, 36.7731, 36.8998, 37.1546, 37.2659, 37.3222, 37.3555, 37.4848, 37.6742, 37.9405, 38.2797, 38.4947, 38.6419, 38.6458, 38.647}
v_r= {.92201, 0.900519, 0.880714, 0.868586, 0.849941, 0.829701, 0.835673, 0.809553, 0.779365, 0.766716, 0.776818, 0.792319, 0.797819, 0.815042, 0.828229, 0.857443, 0.864654, 0.891851, 0.914459, 0.948575, 1.14554, 1.17951, 1.15018, 1.16862, 1.19423, 1.1923, 1.18774, 1.19445, 1.16714, 1.18174, 1.16833, 1.17224, 1.17317, 1.1854, 1.15562, 1.17171, 1.16061, 1.16848, 1.14406, 1.13089, 1.13214, 1.11912, 1.12296, 1.15095, 1.16679, 1.19557, 1.21936, 1.25639, 1.28832, 1.29923, 1.3289, 1.34643, 1.35933, 1.34487, 1.34645, 1.32386, 1.31081, 1.31816, 1.32709, 1.3557, 1.3889, 1.42198, 1.43183, 1.45978, 1.45802, 1.44657, 1.42956, 1.40714, 1.42385, 1.40982, 1.42363, 1.42892, 1.4672, 1.48992, 1.51594, 1.51316, 1.51294, 1.52453, 1.5042, 1.49771, 1.47665, 1.48921, 1.51406, 1.54422, 1.56258, 1.55915, 1.54216, 1.54178, 1.54331, 1.56134, 1.5791, 1.59001, 1.58963, 1.57009, 1.58447, 1.57566, 1.57729, 1.58922, 1.60664, 1.6135, 1.59981, 1.60575, 1.6211, 1.62637, 1.62805, 1.62107, 1.62181, 1.62536, 1.64235, 1.64369, 1.6425, 1.6509, 1.65173, 1.65479, 1.66624, 1.66733, 1.67885, 1.6755, 1.67969, 1.67798, 1.68952, 1.6911, 1.69824, 1.69013, 1.70011, 1.70639, 1.70676, 1.70807, 1.7109, 1.71161, 1.71401, 1.72171, 1.72336, 1.73236, 1.73153, 1.73579, 1.73947, 1.7434, 1.74228, 1.73346, 1.74596, 1.74743, 1.74717, 1.75025, 1.75423, 1.7539, 1.75386, 1.75726, 1.7622, 1.76557, 1.76591, 1.76789, 1.76791, 1.76762, 1.76957, 1.77015, 1.77355, 1.77042, 1.77562, 1.77478, 1.7783, 1.77646, 1.78728, 1.77769, 1.78302, 1.78161, 1.78116, 1.78381, 1.78707, 1.78697, 1.78983, 1.79064, 1.78999, 1.79507, 1.79543, 1.79679, 1.79708, 1.80088, 1.80383, 1.8053, 1.80782, 1.80832, 1.80904, 1.79587, 1.80347, 1.80826, 1.81136, 1.81368, 1.81648, 1.81473, 1.81608, 1.81487, 1.81652, 1.81798, 1.81921, 1.81698, 1.81736, 1.81625, 1.82055, 1.81842, 1.81998, 1.82019, 1.81834, 1.81317, 1.81916, 1.82164, 1.82283, 1.82315, 1.81937, 1.82115, 1.82174, 1.82285, 1.8252, 1.82943, 1.82223, 1.82551, 1.82525, 1.82633, 1.82857, 1.82662, 1.8233, 1.83094, 1.81944, 1.82332, 1.82726, 1.82674, 1.82877, 1.82669, 1.82917, 1.82973, 1.82808, 1.82663, 1.82607, 1.82808, 1.82466, 1.82096, 1.83219, 1.83152, 1.82551, 1.82672, 1.829, 1.82664, 1.82735, 1.82897, 1.82811, 1.82773}

PDV 6 at $z = 229$ mm and $\theta = 90°$ (212 points):
t = {0., 0.02816, 0.0768, 0.13056, 0.16896, 0.20224, 0.22784, 0.27904, 0.30976, 0.37888, 0.4224, 0.51968, 0.58112, 0.64, 0.67328, 0.73216, 0.7936, 0.86016, 0.896, 0.90624, 0.92672, 0.94464, 0.95744, 0.96512, 0.98816, 0.99328, 1.00352, 1.0112, 1.01632, 1.024, 1.02912, 1.03424, 1.03936, 1.0496, 1.0624, 1.1008, 1.14176, 1.15456, 1.24672, 1.27744, 1.35424, 1.39264, 1.45664, 1.48992, 1.56672, 1.60768, 1.65888, 1.73312, 1.8048, 1.85088, 1.89952, 1.93792, 1.95072, 1.9584, 1.96608, 1.97888, 1.984, 1.9968, 2.00192, 2.01984, 2.03776, 2.048, 2.07872, 2.12736, 2.17344, 2.26816, 2.40384, 2.42688, 2.47808, 2.54464, 2.57536, 2.70848, 2.78272, 2.82624, 2.83392, 2.83904, 2.84672, 2.87232, 2.90048, 2.92608, 2.9568, 2.96448, 2.97472, 3.008, 3.08736, 3.16672, 3.22304, 3.25632, 3.31008, 3.36128, 3.40224, 3.4304, 3.55072, 3.60448, 3.63008, 3.64544, 3.67872, 3.69408, 3.74528, 3.75808, 3.88096, 3.92448, 3.96032, 4.05248, 4.09344, 4.13696, 4.32896, 4.42368, 4.48512, 4.55424, 4.59264, 4.65152, 4.7616, 4.91008, 5.02272, 5.08928, 5.19936, 5.23264, 5.312, 5.34272, 5.39648, 5.5168, 5.6704, 5.83424, 5.95456, 6.016, 6.11584, 6.2848, 6.3616, 6.42304, 6.62528, 6.6816, 6.82752, 7.05024, 7.2576, 7.3984, 7.49824, 7.60064, 7.7952, 7.9488, 8.17408, 8.35328, 8.48384, 8.62976, 9.00864, 9.19808, 9.32352, 9.55136, 9.7792, 9.99168, 10.1837, 10.5882, 10.8954, 11.0746, 11.4202, 11.6966, 11.8835, 12.2112, 12.3981, 12.713, 12.8589, 13.0381, 13.1968, 13.3043, 13.4374, 13.6141, 13.7446, 13.911, 14.0314, 14.1696, 14.2848, 14.4666, 14.6893, 14.8454, 15.0144, 15.1936, 15.4598, 15.744, 15.9616, 16.0973, 16.3174, 16.4582, 16.617, 16.7398, 16.8909, 16.937, 17.1059, 17.2467, 17.4336, 17.5974, 17.7178, 17.8637, 17.9302, 18.007, 18.1043, 18.2963, 18.5139, 18.6394, 18.9568, 19.1974, 19.351, 19.6045, 19.9296, 20.1754, 20.4442, 20.6413, 20.9715, 21.3504, 21.9085, 22.3539, 22.4461, 22.4486}
v_r= {0.914397, 0.904267, 0.90077, 0.877393, 0.868072, 0.856896, 0.84844, 0.836751, 0.828272, 0.804628, 0.797952, 0.780647, 0.783826, 0.781018, 0.791071, 0.790357, 0.785601, 0.794082, 0.803051, 0.811465, 0.824512, 0.834475, 0.845974, 0.856738, 0.867111, 0.887186, 1.02551, 0.99814, 1.14173, 1.15177, 1.16158, 1.17039, 1.18027, 1.19598, 1.20702, 1.21364, 1.20389, 1.19985, 1.18797, 1.18224, 1.18155, 1.17126, 1.16354, 1.15202, 1.14193, 1.13164, 1.13967, 1.13775, 1.14491, 1.15475, 1.16517, 1.19673, 1.20318, 1.21135, 1.23035, 1.27108, 1.2895, 1.32175, 1.32771, 1.33895, 1.3495, 1.3583, 1.37259, 1.37053, 1.36715, 1.36011, 1.35365, 1.34398, 1.33333, 1.32489, 1.31417, 1.31055, 1.33042, 1.33972, 1.34711, 1.35703, 1.37891, 1.39532, 1.40624, 1.41616, 1.42261, 1.43204, 1.44475, 1.45684, 1.46647, 1.46412, 1.45317, 1.45593, 1.44871, 1.4429, 1.42929, 1.41891, 1.41298, 1.41919, 1.42957, 1.43989, 1.45094, 1.45841, 1.47233, 1.48064, 1.51572, 1.51031, 1.52229, 1.52353, 1.51404, 1.50631, 1.48543, 1.49442, 1.50566, 1.52678, 1.53774, 1.5481, 1.55838, 1.55565, 1.53849, 1.53471, 1.5372, 1.54849, 1.55851, 1.56918, 1.58019, 1.58907, 1.5795, 1.57349, 1.5823, 1.5885, 1.60407, 1.60961, 1.60233, 1.60314, 1.6005, 1.61141, 1.62209, 1.62293, 1.62277, 1.63206, 1.64174, 1.6398, 1.63847, 1.64424, 1.65383, 1.65163, 1.6587, 1.66387, 1.66932, 1.67588, 1.67688, 1.67781, 1.68168, 1.68555, 1.69049, 1.69584, 1.70082, 1.70381, 1.70996, 1.71307, 1.71628, 1.72113, 1.72612, 1.72447, 1.7269, 1.73352, 1.73637, 1.73396, 1.73929, 1.74102, 1.74239, 1.74173,

1.737, 1.74425, 1.74967, 1.74864, 1.74712, 1.74743, 1.75482, 1.75887, 1.75974, 1.76094, 1.76484, 1.76587, 1.76473, 1.76804, 1.76883, 1.77666, 1.76965, 1.7746, 1.77569, 1.78349, 1.78445, 1.78494, 1.78722, 1.7871, 1.78028, 1.78469, 1.78638, 1.78843, 1.78923, 1.78943, 1.79294, 1.79578, 1.79301, 1.79717, 1.79924, 1.8, 1.79991, 1.80315, 1.80123, 1.80555, 1.80699, 1.80759, 1.8084, 1.80829}

PDV 7 at $z = 229$ mm and $\theta = 180^\circ$ (223 points):
t = {0., 0.07936, 0.13568, 0.18944, 0.22784, 0.23808, 0.27136, 0.32768, 0.36608, 0.42752, 0.49664, 0.5504, 0.64512, 0.6784, 0.74752, 0.82944, 0.91648, 0.9344, 0.96768, 0.99072, 1.04448, 1.05216, 1.06752, 1.09824, 1.10592, 1.11616, 1.14176, 1.14688, 1.16992, 1.20832, 1.2416, 1.26208, 1.28, 1.30816, 1.37216, 1.408, 1.44384, 1.47456, 1.50016, 1.51808, 1.52576, 1.5488, 1.55904, 1.58208, 1.61024, 1.62304, 1.66656, 1.7536, 1.7664, 1.80224, 1.8304, 1.83808, 1.8432, 1.856, 1.86624, 1.87392, 1.88928, 1.91232, 1.92768, 1.93536, 1.95584, 1.96608, 1.97376, 1.984, 1.99424, 2.04032, 2.048, 2.05312, 2.05824, 2.06592, 2.10432, 2.16576, 2.21184, 2.23488, 2.24768, 2.26816, 2.28608, 2.30912, 2.33728, 2.34752, 2.36544, 2.39872, 2.40896, 2.43968, 2.46272, 2.47552, 2.50624, 2.56512, 2.62912, 2.67776, 2.688, 2.71104, 2.71616, 2.75712, 2.79808, 2.80832, 2.81344, 2.83392, 2.86208, 2.88768, 2.9184, 2.94912, 2.96704, 2.97472, 2.99776, 3.10016, 3.20768, 3.22048, 3.2384, 3.27168, 3.2768, 3.31264, 3.36896, 3.42528, 3.46368, 3.5456, 3.62496, 3.66592, 3.68896, 3.70944, 3.72736, 3.77856, 3.8272, 3.90656, 3.96288, 4.01664, 4.0704, 4.09344, 4.10624, 4.13952, 4.1472, 4.16512, 4.22144, 4.27264, 4.34176, 4.38272, 4.44928, 4.5056, 4.55168, 4.62336, 4.70272, 4.83584, 4.89472, 4.93312, 4.98176, 5.05088, 5.14048, 5.18656, 5.32736, 5.37856, 5.43744, 5.55264, 5.72928, 5.888, 5.94176, 5.9904, 6.1568, 6.30784, 6.39744, 6.59968, 6.71488, 6.8096, 6.90944, 7.05024, 7.24224, 7.3728, 7.63136, 7.77216, 7.88224, 8.064, 8.256, 8.4608, 8.6656, 8.84224, 8.9728, 9.18272, 9.36448, 9.7664, 10.0531, 10.2758, 10.6342, 10.9235, 11.1898, 11.4022, 11.561, 11.7325, 11.8349, 12.0269, 12.1856, 12.3315, 12.6464, 12.8154, 13.1763, 13.5603, 13.8419, 14.2131, 14.4282, 14.633, 14.8045, 14.871, 15.0042, 15.1219, 15.2474, 15.3677, 15.5264, 15.7491, 15.9411, 16.1075, 16.4147, 16.7373, 17.1648, 17.5232, 18.1555, 18.5856, 18.7546, 19.0515, 19.3024, 19.6326, 19.8835, 20.1626, 20.7334, 20.8154, 20.8179}
v_r = {0.895259, 0.890997, 0.87805, 0.863257, 0.864812, 0.848741, 0.845812, 0.83487, 0.817608, 0.806105, 0.791859, 0.786172, 0.774748, 0.792669, 0.790131, 0.798479, 0.818675, 0.825583, 0.841117, 0.850422, 1.14902, 1.16547, 1.18917, 1.19206, 1.19596, 1.18804, 1.17434, 1.18652, 1.21053, 1.19436, 1.19787, 1.18677, 1.18958, 1.18829, 1.18384, 1.17111, 1.161, 1.16629, 1.14373, 1.1438, 1.14587, 1.15831, 1.15042, 1.14197, 1.13145, 1.1465, 1.1399, 1.14566, 1.15649, 1.16915, 1.16095, 1.15247, 1.17164, 1.18488, 1.16243, 1.16569, 1.16387, 1.17792, 1.19193, 1.19109, 1.207, 1.21948, 1.23689, 1.25389, 1.27107, 1.2751, 1.28768, 1.30308, 1.31747, 1.34365, 1.36464, 1.35132, 1.33967, 1.3496, 1.35512, 1.35629, 1.34475, 1.35859, 1.35451, 1.3424, 1.35566, 1.35402, 1.34283, 1.34695, 1.34372, 1.32855, 1.32176, 1.31705, 1.31062, 1.3142, 1.32914, 1.33376, 1.32023, 1.32869, 1.36089, 1.36593, 1.35822, 1.38038, 1.39201, 1.41023, 1.41213, 1.41527, 1.42465, 1.44104, 1.45109, 1.45628, 1.44032, 1.44105, 1.44869, 1.44362, 1.43405, 1.4272, 1.43322, 1.43222, 1.41995, 1.42633, 1.42628, 1.47464, 1.45423, 1.46793, 1.48561, 1.49049, 1.50783, 1.51941, 1.52163, 1.5336, 1.52239, 1.50831, 1.50219, 1.53424, 1.5177, 1.49381, 1.50749, 1.49356, 1.49653, 1.51252, 1.50178, 1.51735, 1.52882, 1.54854, 1.55471, 1.5545, 1.55471, 1.53722, 1.54336, 1.53422, 1.57042, 1.57549, 1.5853, 1.5913, 1.5808, 1.5829, 1.58383, 1.59067, 1.60782, 1.61461, 1.6121, 1.60513, 1.61725, 1.6222, 1.63079, 1.62506, 1.62322, 1.6333, 1.64676, 1.64281, 1.64653, 1.64972, 1.65923, 1.66197, 1.66284, 1.66985, 1.66944, 1.67933, 1.67596, 1.68344, 1.68835, 1.6936, 1.69882, 1.70392, 1.70427, 1.7106, 1.71253, 1.72483, 1.7178, 1.71915, 1.71789, 1.72452, 1.72579, 1.72964, 1.73475, 1.73808, 1.74168, 1.74391, 1.74512, 1.74923, 1.75295, 1.74907, 1.74909, 1.75452, 1.75828, 1.75631, 1.75545, 1.75905, 1.75896, 1.75732, 1.76083, 1.76218, 1.76148, 1.76401, 1.76587, 1.76879, 1.7673, 1.76601, 1.76407, 1.76745, 1.76582, 1.76629, 1.76591, 1.76694, 1.76697}

PDV 8 at $z = 229$ mm and $\theta = 270^\circ$ (212 points):
t = {0., 0.08192, 0.1536, 0.21504, 0.22528, 0.3072, 0.35584, 0.40448, 0.4736, 0.512, 0.5632, 0.60672, 0.69632, 0.7424, 0.78848, 0.87296, 0.88576, 0.896, 0.92672, 0.96, 0.9728, 0.97792, 0.98304, 0.99072, 1.01632, 1.024, 1.06752, 1.1008, 1.13408, 1.1648, 1.18528, 1.19808, 1.24416, 1.31328, 1.35424, 1.4208, 1.46432, 1.52576, 1.5744, 1.60512, 1.66912, 1.72032, 1.76384, 1.82528, 1.87136, 1.8944, 1.91488, 1.92512, 1.93024, 1.9456, 1.9584, 1.97376, 1.97888, 1.984, 1.99168, 2.00192, 2.04544, 2.07104, 2.11712, 2.15808, 2.21696, 2.27584, 2.33216, 2.41152, 2.46528, 2.5216, 2.6624, 2.75968, 2.7776, 2.80064, 2.81088, 2.81856, 2.83904, 2.85952, 2.88768, 2.89536, 2.92608, 2.94912, 2.9696, 2.99776, 3.11808, 3.24608, 3.29216, 3.37408, 3.4432, 3.47904, 3.58656, 3.63008, 3.68384, 3.7376, 3.7632, 3.82976, 3.85792, 3.89632, 3.95776, 4.04992, 4.09856, 4.15488, 4.25984, 4.43136, 4.44672, 4.47232, 4.5184, 4.56704, 4.64896, 4.75136, 4.83584, 4.90496, 4.9408, 5.12768, 5.20192, 5.23776, 5.30432, 5.36064, 5.44, 5.56032, 5.68064, 5.7728, 5.8496, 5.90848, 5.98272, 6.06976, 6.15424, 6.28736, 6.4128, 6.56384, 6.64064, 6.73536, 6.87616, 7.0528, 7.23968, 7.31392, 7.488, 7.6416, 7.91296, 8.01536, 8.16384, 8.35072, 8.576, 8.84224, 9.05728, 9.19552, 9.46432, 9.7152, 10.0941, 10.4269, 10.839, 11.2538, 11.817, 12.329, 12.585, 13.0048, 13.4528, 13.7754, 13.9776, 14.2746, 14.7763, 15.0912, 15.7133, 16.3456, 16.5837, 16.8525, 17.2928, 17.6435, 17.9686, 18.9056, 19.6659, 20.2496, 20.6003, 20.9178, 21.2147, 21.4989, 21.6678, 21.7242, 21.7933, 21.8829, 22.0518, 22.2976, 22.5997, 22.9094, 23.744, 24.448, 24.681, 25.3978, 26.327, 27.1027, 27.6838, 28.0243, 28.5619, 28.9075, 29.4477, 29.9213, 30.3616, 30.8198, 31.1424, 31.4726, 31.8362, 32.2589, 32.2355, 32.489, 32.9907, 33.5206, 34.0506, 34.7699, 35.3101, 36.0499, 36.8154, 37.4605, 38.0186, 38.2208, 38.2259}
v_r = {0.883774, 0.885136, 0.870253, 0.85972, 0.857212, 0.83732, 0.815379, 0.804163, 0.794804, 0.791107, 0.775318, 0.765931, 0.772061, 0.7813, 0.786447, 0.794934, 0.804023, 0.814747, 0.82615, 0.839588, 0.845464, 0.865661, 0.911652, 0.941452, 1.165, 1.1904, 1.19983, 1.19038, 1.18913, 1.17269, 1.18596, 1.18554, 1.19572, 1.19502, 1.18444, 1.17488, 1.16231, 1.15218, 1.14119, 1.13022, 1.12698, 1.13023, 1.14139, 1.15051, 1.16246, 1.17255, 1.18246, 1.19131, 1.19755, 1.21559, 1.22377, 1.23638, 1.24627, 1.26494, 1.30572, 1.34757, 1.36102, 1.37223, 1.37547, 1.36742, 1.36336, 1.35379, 1.36473, 1.33593, 1.33383, 1.32238, 1.31176, 1.31566, 1.32578, 1.33605, 1.3458, 1.35625, 1.37044, 1.38239, 1.39083, 1.39997, 1.4264, 1.43615, 1.44677, 1.45977, 1.46839, 1.45786, 1.44765, 1.43604, 1.42518, 1.41455, 1.41798, 1.42838, 1.43825, 1.47229, 1.48346, 1.49472, 1.50599, 1.51721, 1.52881, 1.52231, 1.51138, 1.50538, 1.48938, 1.48795, 1.49813, 1.50564, 1.52063, 1.52481, 1.5493, 1.56067, 1.55729, 1.55215, 1.54703, 1.53568, 1.5467, 1.55706, 1.56805, 1.57692, 1.58613, 1.58461, 1.57862, 1.5679, 1.57237, 1.57869, 1.59051, 1.60173, 1.60845, 1.60718, 1.60094, 1.59909, 1.60633, 1.62128, 1.62926, 1.62144, 1.62014, 1.6319, 1.64327, 1.64177, 1.64386, 1.65212, 1.65798, 1.65357, 1.6623, 1.66966, 1.6673, 1.67668, 1.68024, 1.68346, 1.68781, 1.69656, 1.69934, 1.70753, 1.71616, 1.72479, 1.72804, 1.7337, 1.73911, 1.74142, 1.74534, 1.74954, 1.75581, 1.75803, 1.76318, 1.7676, 1.77176, 1.77283, 1.77466, 1.77831, 1.77868, 1.78273, 1.78637, 1.78829, 1.79128, 1.79041, 1.79051, 1.79173, 1.78783, 1.79497, 1.79174, 1.79465, 1.79338, 1.79517, 1.79682, 1.79838, 1.7987, 1.80168, 1.80616, 1.80945, 1.8078, 1.80525, 1.80669, 1.80977, 1.8105, 1.81148, 1.81157, 1.81376, 1.81635, 1.81712, 1.81906, 1.82048, 1.81917, 1.82073, 1.82215, 1.82196, 1.82216, 1.82245, 1.82453, 1.82539, 1.8247, 1.82484, 1.82493, 1.82534, 1.82584, 1.82607, 1.82516, 1.82454}